

Residual stress effects on fatigue crack growth rate of mild steel S355 exposed to air and seawater environments

Xin, Haohui; Veljkovic, Milan

DOI

[10.1016/j.matdes.2020.108732](https://doi.org/10.1016/j.matdes.2020.108732)

Publication date

2020

Document Version

Final published version

Published in

Materials and Design

Citation (APA)

Xin, H., & Veljkovic, M. (2020). Residual stress effects on fatigue crack growth rate of mild steel S355 exposed to air and seawater environments. *Materials and Design*, 193, Article 108732. <https://doi.org/10.1016/j.matdes.2020.108732>

Important note

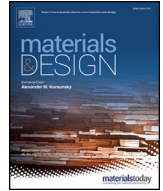
To cite this publication, please use the final published version (if applicable). Please check the document version above.

Copyright

Other than for strictly personal use, it is not permitted to download, forward or distribute the text or part of it, without the consent of the author(s) and/or copyright holder(s), unless the work is under an open content license such as Creative Commons.

Takedown policy

Please contact us and provide details if you believe this document breaches copyrights. We will remove access to the work immediately and investigate your claim.



Residual stress effects on fatigue crack growth rate of mild steel S355 exposed to air and seawater environments

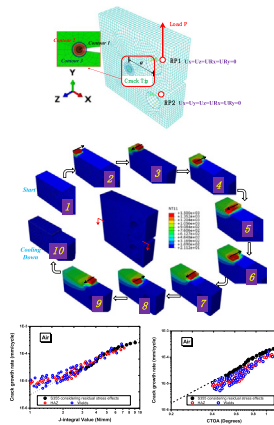
Haohui Xin^{*}, Milan Veljkovic

Faculty of Civil Engineering and Geosciences, Delft University of Technology, Netherlands

HIGHLIGHTS

- The parameters of fatigue crack growth rate exposed to air and seawater were presented.
- Fatigue crack growth rate were predicted using SIF, J-integral, CTOD and CTOA.
- Effect of the residual stresses on the fatigue crack growth rate is investigated.

GRAPHICAL ABSTRACT



ARTICLE INFO

Article history:

Received 22 September 2019
 Received in revised form 14 March 2020
 Accepted 15 April 2020
 Available online 5 May 2020

Keywords:

Fatigue crack growth rate
 Residual stress
 J-integral
 Crack tip opening displacement (CTOD)
 Crack tip opening angle (CTOA)

ABSTRACT

In this paper, the parameters of fatigue crack growth rate for Q355J2 steel exposed to air and seawater were presented using the "Paris' law" based on the stress intensity factor (SIF), J-integral, crack tip opening displacement (CTOD) and crack tip opening angle (CTOA). The residual stress of a compact tension specimen is analysed by modelling of the welding process based on subsequently thermal mechanical stress analysis. Effect of the residual stresses on the fatigue crack growth rate is investigated by considering the numerically predicted residual stress distribution due to welding. The fatigue crack growth rate based on the parent material considering residual stress effects is compared with welds and the heat affected zone (HAZ).

© 2020 The Author(s). Published by Elsevier Ltd. This is an open access article under the CC BY license (<http://creativecommons.org/licenses/by/4.0/>).

1. Introduction

The general offshore towers for wind industry are mostly constructed with relatively thick tubular steel shells to prevent local buckling, see empirical formula depending on the diameter in [1]. The offshore structures are exposed to harsh environment with constant

^{*} Corresponding author.
 E-mail address: H.Xin@tudelft.nl (H. Xin).

Nomenclature

a	crack length
B	specimen thickness
CTOD	Crack tip opening displacement
CTOA	Crack tip opening angle
E	Young's modulus
G	Griffith energy release rate
J	J-integral
K	stress intensity factor
ΔK	stress intensity factor range
K_{\max}	The maximum stress intensity factor during a fatigue loading cycle
K_{\min}	the minimum stress intensity factor during a fatigue loading cycle
P	applied load
W	specimen width
C_K, m_K	Paris law fatigue crack growth rate parameters based on stress intensity factor
C_J, m_J	Paris law fatigue crack growth rate parameters based on J-integral
C_{δ}, m_{δ}	Paris law fatigue crack growth rate parameters based on CTOD
C_{ψ}, m_{ψ}	Paris law fatigue crack growth rate parameters based on CTOA
ν	Poisson's ratio

exertion of wave and wind forces leading to fatigue and corrosion damage. The fatigue crack growth rate of offshore structures needs to be characterized in air and seawater environments in order to reliably predict the remaining fatigue life [2–4]. The fatigue phenomenon is the process of progressive localized permanent structural change occurring in a material under cyclic loading, studied also in [5–10]. The fatigue process of steel structures is divided into two stages: fatigue crack initiation period and fatigue crack propagation period.

Welding is one of the most important technologies to connect the structure made of steel plates rolled into the cylindrical structure for supporting the offshore wind turbines. The locally introduced heat either in the longitudinal or in the circumferential direction due to the welding causes an abrupt temperature increase, followed by subsequent cooling to the environment temperature. This process leads to residual stress because of the restrained shrinkage of the heated zone by surrounded cooler zone [11–14]. The residual stresses induced by welding process have a significant impact on both fatigue crack initiation and fatigue crack propagation [15]. The authors [15] investigated the residual stress on fatigue crack initiation of butt-welded plates made of high strength steels. The results showed that the residual stress influence the fatigue crack initiation position and the fatigue behaviour of butt-welded plate. The numerically defined residual stress show better agreement with results obtained in fatigue tests than the residual stress-free model. The effective value of the stress intensity factor may differ significantly depending if [16] a residual stress are considered or not. The research of residual stress effects on fatigue crack initiation and propagation is of highly practical significance [17–19].

Current research on fatigue crack growth prediction of welded connections mainly use linear elastic fracture mechanics (LEFM)-based Paris' law fitted to fatigue tests [2–4]. In terms of fatigue crack propagation driving force of LEFM, fracture toughness [20], the stress intensity factor K (SIF) [21] or the elastic energy release rate G [22] is the most important parameter. Griffith [23] in 1920, proposed the energy theory to describe the fracture of brittle materials. Irwin [22] further modified the energy theory in 1956 and employed the energy release rate G to measure the energy for crack extension increment. The stress intensity

factor K was introduced by Irwin [21] to describe the intensity of elastic crack-tip fields, which is the fundamental parameter of the linear elastic fracture mechanics (LEFM). In terms of fatigue crack propagation from the fatigue experiments, Paris et al. [24] proposed a fatigue crack growth rate equation that link the stress intensity factor range ΔK to sub-critical fatigue crack growth rate da/dN , known as "Paris' law". Nowadays, the Paris' law and its extensions [25–29] are widely used to predict the fatigue crack growth for different engineering structures [30]. The commercial software ABAQUS [31] includes, in the direct cyclic approach module, the extended finite element method (XFEM) [32]. It predicts the fatigue crack growth using Paris' law based on Griffith energy rate (G) and the virtual crack closure techniques (VCCT) based on the LEFM.

However, the residual stress influences stress concentration and, in combination with the external loading, causes yielding close to the welding zone [14]. A plastic zone is caused by residual stress and the crack tip blunted. The residual stresses induced by welding process in the plastic wake lead to plasticity-induced fatigue crack closure. The residual stretch in the plastic wake causes the crack faces to close at a positive remote stress. Thus, the SIF-based Paris' law under the principal of LEFM may not be suitable to predict the fatigue crack growth of welded joints with plasticity considering the residual stress. In order to consider the local plasticity introduced by the residual stress, the fatigue crack propagation driving force needed to be considered carefully. For elastic-plastic crack propagation, due to slow and stable micro ductile void growth and coalescence, the fracture toughness is often described as crack-tip opening displacement δ (CTOD), or J-integral, or crack tip opening angle (CTOA). Wells [33] at the British Welding Institute proposed, already in 1963, proposed the CTOD in order to extend the elastic stress intensity factor approach into situation at and beyond yielding. The CTOD criteria defines that the crack propagation when a critical δ_c in the structure is met or exceeded similar to SIF criteria, i.e. $\delta \geq \delta_c$. Rice [33] proposed the J-integral to characterize the intensity of elastic-plastic crack-tip fields in 1968, which leads to the elastic-plastic fracture mechanics (EPFM). For plasticity deformation, the J-integral \bar{J} is independent of the path integration around the crack tip

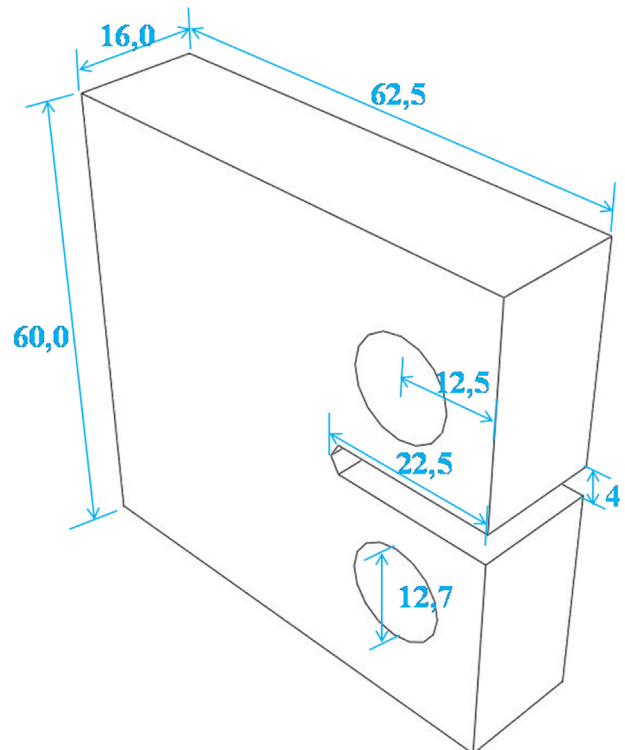


Fig. 1. Dimensions of compact tension specimen (unit: mm).

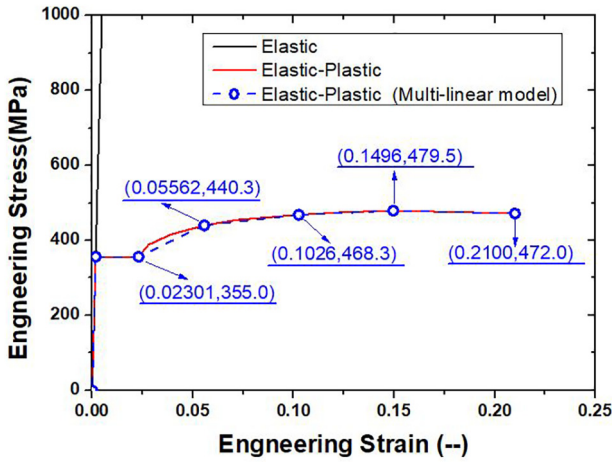


Fig. 2. Stress-strain relationship of S355 steel used to calculate fracture toughness.

for both theoretical validation [34,35] and finite element simulation [36]. The concept of crack tip opening angle was introduced by Anderson [36] to simulate the stable crack extension behaviour by finite element (FE) method. The angle ψ between two crack surfaces was employed as the crack growth criterion.

The welding process is quite complicated and the grain microstructures of heat affected zone and welds changed during welding. The experimental driven strategies to investigate the fatigue crack propagation behaviour of welded steel joints with complicated geometry is time consuming. This paper aims to discuss a relative simple engineering approach by neglecting the phase transformation effects, and to evaluate whether it is possible to predict the fatigue crack growth rate of welded joints based on the parent material in the situation that fatigue experiments are unavailable. Residual stresses of complicated geometry welded steel structures is numerically predicted because it is very costly to measure them. The parameters of the "Paris' law" C and m , for fatigue crack growth rate of Q355J2 steel grade exposed to air and seawater environments were derived using experimental results [3] and finite element simulation based on SIF, J-integral, CTOD and CTOA. The residual stress of a compact tension specimen is analysed by modelling of the welding process based on subsequently thermal mechanical stress

analysis and kill/birth strategies. The residual stress effect on the fatigue crack growth rate is investigated by considering the numerically predicted residual stress distribution due to welding. The fatigue crack growth rate based on parent material is compared with the experimental fatigue crack growth rate of welds and the heat affected zone (HAZ).

2. Fatigue crack propagation based on different fracture parameters

The fracture toughness, including SIF " K ", J-integral \bar{J} , CTOD " δ " and CTOA " ψ " were numerically calculated using commercially available finite element software ABAQUS [31]. The geometry of the compact tension specimen is shown in Fig. 1. The detailed fatigue crack growth rate of material exposed to air and seawater environment of a monopile used in the offshore structures were reported in [3]. The relationships between SIF and J-integral, SIF and CTOD, SIF and CTOA, respectively are fitted through validated numerical simulation. The "SIF-based Paris' law" under the principle of LEFM through fatigue tests were further converted to J-integral based, CTOD based and CTOA based "Paris' law" using the EPFM. The engineering stress-strain curve of the parent material S355 used to calculate the fracture toughness is shown in Fig. 2.

2.1. SIF-based fatigue crack propagation rate

As is shown in Fig. 3, the conventional implicit finite element method in the ABAQUS [31] are used to obtain fracture parameters in this section based on contour integral. The Young's modulus is set as 210.0GPa and the Poisson's ratio is set to 0.3. C3D8 elements are used in all models. For linear elastic isotropic material and the square root singularity, the mid-side node parameter is defined as 0.25, the collapsed element side is selected as "single node". Three contours are used in the analysis. Two reference points, namely RP1 and RP2, are assigned to the centre of the holes in the middle of CT specimen. The reference points are connected to the compact tension specimens through MPC constraints. Translations in X- and Z-direction, and rotations around X- and Y-axes of RP1 are fixed, while translations in X-, Y-, Z-direction, and rotations around X-, Y-axes of RP2 are fixed. The external load P is applied at the RP1. The crack length varied from $a = 20$ mm to $a = 35$ mm to analyse SIF values. The self-contact is used to consider the crack closure with "hard" along the normal direction and "frictionless" along the tangential direction.

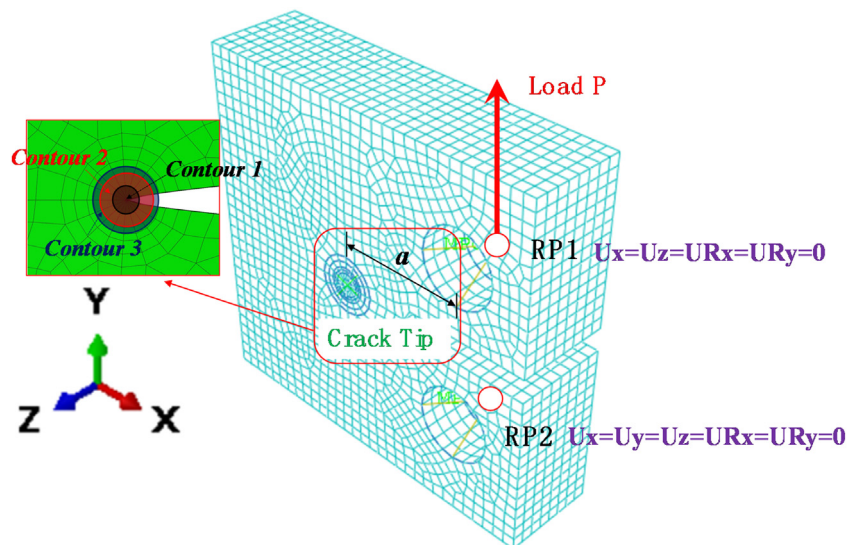


Fig. 3. Finite element model of compact tension specimens ($a = 20$ mm).

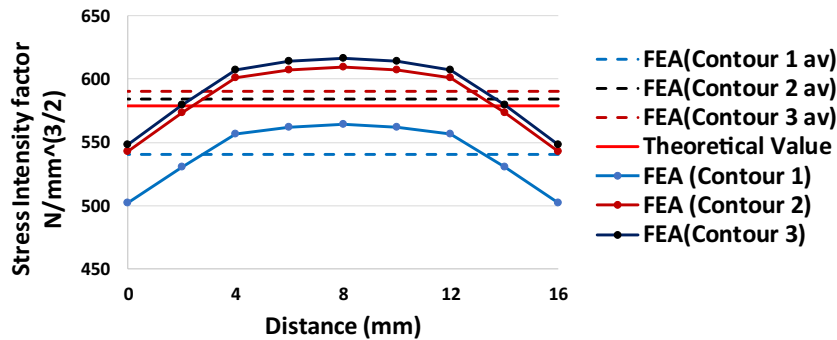
Table 1
SIF comparisons between FE and theoretical value using LEFM with applied load $P = 9\text{kN}$.

Crack length (mm)	Contour-3-av (N/mm ^{1.5})	Contour-3-Max (N/mm ^{1.5})	Contour-3-Min (N/mm ^{1.5})	Theoretical value (N/mm ^{1.5})	Average/Theoretical	Max/Min
a = 20	590.3	616.2	547.8	579.1	1.02	1.12
a = 21	620.1	647.5	575.1	610.8	1.02	1.13
a = 22	652.6	681.8	604.9	645.1	1.01	1.13
a = 23	688.4	719.3	637.8	682.5	1.01	1.13
a = 24	727.6	760.5	673.9	723.4	1.01	1.13
a = 25	771.4	806.4	714.3	768.4	1.00	1.13
a = 26	819.3	856.6	758.3	818.3	1.00	1.13
a = 27	873.6	913.6	808.4	873.8	1.00	1.13
a = 28	934.0	976.9	864.0	936.1	1.00	1.13
a = 29	1002.8	1048.8	927.4	1006.4	1.00	1.13
a = 30	1081.0	1130.8	999.4	1086.2	1.00	1.13
a = 31	169.4	1223.5	1080.7	1177.4	1.04	1.13
a = 32	1271.4	1330.5	1174.5	1282.4	0.99	1.13
a = 33	1387.7	1452.4	1281.2	1404.2	0.99	1.13
a = 34	1525.8	1597.4	1407.9	1546.5	0.99	1.13
a = 35	1684.3	1764.1	1552.6	1714.4	0.98	1.14

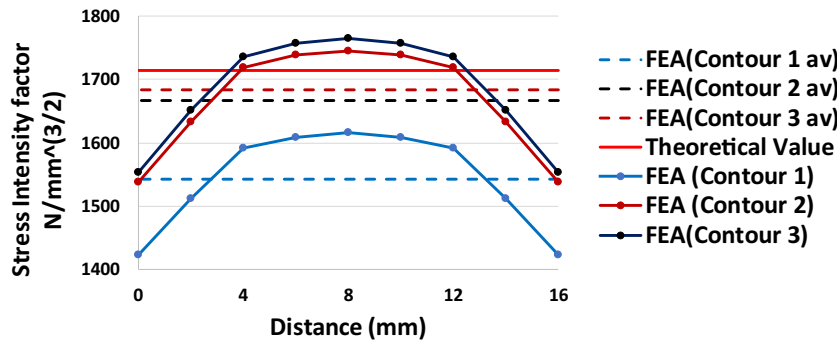
The SIF results obtained from FE simulation are compared to theoretical values for different crack length and a constant applied load, see Table 1. The typical SIF distribution along the thickness direction with a crack length $a = 20\text{ mm}$ and $a = 35\text{ mm}$ under the external load $P = 9\text{ kN}$ is shown in Fig. 4. The SIFs calculated from the first contour tend to be smaller than from other contours. The SIF difference between the second and the third contour is rather small. The SIFs from the third contour are used for the fatigue crack growth rate in this paper. The SIF calculated at the mid-thickness is larger than on the sides. The ratio between maximum and minimum SIF is between 1.12 and 1.14.

The SIF ranges during fatigue crack growth rate tests are usually calculated based on Eqs. (1)–(3) [37,38]. The FE simulation is verified comparing the theoretical SIFs to the SIF calculated from the average third contour integral, as shown in Table 1 and Fig. 4. The difference between theoretical and FE SIFs is within 4%, indicating that FE model is suitable for the fatigue crack propagation prediction.

$$\Delta K = K_{\max} - K_{\min} \tag{1}$$



(a) $a = 20\text{ mm}$



(b) $a = 35\text{ mm}$

Fig. 4. Typical SIF distribution along thickness direction (LEFM) with $P = 9\text{ kN}$.

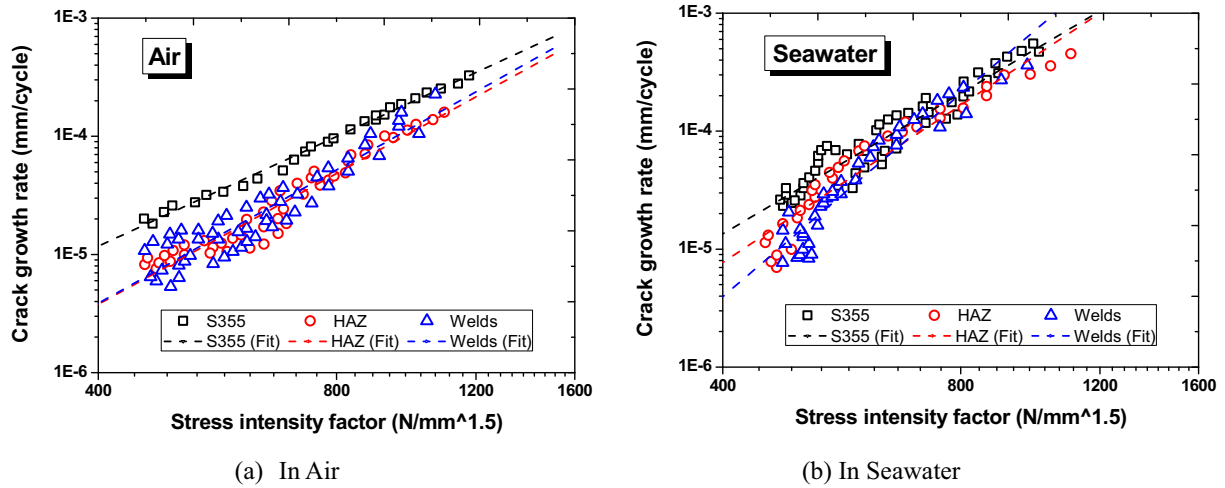


Fig. 5. Fatigue crack growth rate based on SIF in different environment.

$$K = \frac{P}{B\sqrt{W}} f\left(\frac{a}{W}\right) \quad (2)$$

$$f\left(\frac{a}{W}\right) = \frac{\left(2 + \frac{a}{W}\right)}{\left(1 - \frac{a}{W}\right)^{3/2}} \left[0.886 + 4.64\left(\frac{a}{W}\right) - 13.32\left(\frac{a}{W}\right)^2 + 14.72\left(\frac{a}{W}\right)^3 - 5.60\left(\frac{a}{W}\right)^4 \right] \quad (3)$$

The fatigue crack growth rates of parent steel material, HAZ, and welds in different environments are reproduced from the literature [3], see Fig. 5 and Table 2. The fatigue crack growth rate parameters C_k

and m_k of the “SIF-based Paris law” are fitted using the test results. The fitted results are listed in Table 2. The exponent m_k of welds and HAZ is larger than m_k of the parent material. The exponent m_k in the seawater is larger than it in the air.

$$\frac{d\alpha}{dN} = C_k (\Delta K)^{m_k} \quad (4)$$

2.2. J-integral based fatigue crack propagation rate

The same finite element models, used to calculate SIFs, are suitable to calculate the J-integral according to LEFM and EPFM. The crack tip singularity is material behaviour dependent. For plastic large-strain localized deformation, the crack tip is not perfectly sharp and a blunted notch is proposed to consider the plastic zone ahead the crack tip. Thus, the mid-side node parameter is defined as 0.25, and the collapsed element side with “double node” for the combined square root and “1/r” singularity.

The J-integrals calculated by FEM assuming LEFM and EPFM approach are summarized in Tables 3 and 4 respectively. The typical J-integrals distribution along the thickness direction with a crack length $a = 20$ mm and $a = 35$ mm under the external load $P = 9$ kN is shown in Figs. 6 and 7, respectively. The J-integrals from the first

Table 2
SIF based fatigue crack propagation rate parameters using LEFM.

Environment	Material	P (kN)	R-ratio	C_k	m_k	R-square
Air	Steel (S355)	9.0	0.1	1.125×10^{-13}	3.082	0.99
	HAZ	9.0	0.1	1.021×10^{-15}	3.678	0.93
	Welds	9.0	0.1	6.622×10^{-16}	3.753	0.89
Seawater	Steel (S355)	9.0	0.1	6.699×10^{-16}	3.960	0.91
	HAZ	9.0	0.1	2.244×10^{-17}	4.433	0.92
	Welds	9.0	0.1	5.272×10^{-21}	5.717	0.91

Table 3
J-integral (LEFM) comparisons between FE and theoretical results with $P = 9$ kN.

Crack length (mm)	Contour-3-av (N·mm)	Contour-3-Max (N·mm)	Contour-3-Min (N·mm)	Theoretical (N.mm)		Average/Theoretical		Max/Min
				Plane stress	Plane strain	Plane stress	Plane strain	
a = 20	1.55	1.66	1.38	1.60	1.45	0.97	1.07	1.20
a = 21	1.71	1.84	1.52	1.78	1.62	0.96	1.06	1.21
a = 22	1.89	2.04	1.68	1.98	1.80	0.95	1.05	1.21
a = 23	2.11	2.27	1.87	2.22	2.02	0.95	1.04	1.21
a = 24	2.36	2.54	2.08	2.49	2.26	0.95	1.04	1.22
a = 25	2.65	2.86	2.34	2.81	2.56	0.94	1.04	1.22
a = 26	2.99	3.22	2.64	3.18	2.90	0.94	1.03	1.22
a = 27	3.40	3.67	3.00	3.64	3.31	0.93	1.03	1.22
a = 28	3.89	4.20	3.43	4.17	3.79	0.93	1.03	1.22
a = 29	4.49	4.84	3.95	4.82	4.39	0.93	1.02	1.23
a = 30	5.22	5.63	4.60	5.62	5.11	0.93	1.02	1.22
a = 31	6.11	6.59	5.38	6.60	6.00	0.93	1.02	1.22
a = 32	7.23	7.81	6.37	7.83	7.13	0.92	1.01	1.23
a = 33	8.62	9.32	7.58	9.39	8.54	0.92	1.01	1.23
a = 34	10.44	11.29	9.17	11.39	10.36	0.92	1.01	1.23
a = 35	12.74	13.78	11.18	13.99	12.74	0.91	1.00	1.23

Table 4
J-integral (EPFM) comparisons between FE and theoretical results with P = 9 kN.

Crack length (mm)	Contour-3-av (N·mm)	Contour-3-Max (N·mm)	Contour-3-Min (N·mm)	Theoretical (N.mm)		Average/Theoretical		Max/Min
				Plane stress	Plane strain	Plane stress	Plane strain	
a = 20	1.60	1.72	1.40	1.60	1.45	1.00	1.10	1.23
a = 21	1.77	1.91	1.55	1.78	1.62	0.99	1.09	1.23
a = 22	1.96	2.12	1.71	1.98	1.80	0.99	1.09	1.24
a = 23	2.19	2.37	1.90	2.22	2.02	0.99	1.08	1.25
a = 24	2.45	2.65	2.12	2.49	2.27	0.98	1.08	1.25
a = 25	2.76	3.00	2.39	2.81	2.56	0.98	1.08	1.26
a = 26	3.13	3.40	2.69	3.19	2.90	0.98	1.08	1.26
a = 27	3.57	3.89	3.05	3.64	3.31	0.98	1.08	1.28
a = 28	4.10	4.48	3.47	4.17	3.79	0.98	1.08	1.29
a = 29	4.77	5.22	3.97	4.82	4.39	0.99	1.09	1.31
a = 30	5.59	6.16	4.55	5.62	5.11	0.99	1.09	1.35
a = 31	6.63	7.36	5.25	6.60	6.00	1.00	1.11	1.40
a = 32	7.95	8.91	6.11	7.83	7.13	1.02	1.12	1.46
a = 33	9.70	10.98	7.22	9.39	8.54	1.03	1.14	1.52
a = 34	12.34	14.18	8.81	11.39	10.36	1.08	1.19	1.61
a = 35	17.20	20.25	11.59	14.00	12.74	1.23	1.35	1.75

contour tend to be smaller than from other contours in LEFM simulation. The J-integrals from the first contour is larger than from other contours with a = 20 mm and is smaller than other contours with a = 35 mm EPFM simulation. The J-integral difference between the second and the third contour is quite small. The J-integrals from the third contour are used for the fatigue crack growth rate in this paper as they are perceived as the accurate (consistent) prediction. The J-integrals at the mid-thickness is larger than at the sides. The ratio between maximum and minimum J-integrals is between 1.20 and 1.23 in LEFM simulation, but the ratio between maximum and minimum J-integrals increased a lot with the crack length increase, ranging from 1.23 to 1.75 in EPFM simulation. The deformation comparisons between LEFM and EPFM with crack length a = 20 mm and under external load P = 9kN is shown in Fig. 8. The crack tip is very sharp using LEFM while the crack shape is relatively blunt in EPFM approach.

For linear elastic materials, $J_{el} = G$, the relationship between K and J is obtained according to Eq. (5). The comparisons between theoretical J_{el} and FE simulation are listed in Tables 3 and 4. The ratio between FE (LEFM) and theoretical values (plane stress) is from 0.91 to 0.97, between FE (LEFM) and theoretical values (plane strain) is from 1.00 to 1.07. The ratio between FE (EPFM) and theoretical values (plane stress) is from 0.98 to 1.23, between FE (EPFM) and theoretical values (plane strain) is from 1.23 to 1.75.

$$J_{el} = G = \frac{K^2}{E'} \tag{5}$$

Where $E' = E$ for plane stress conditions, $E' = E/(1 - \nu^2)$ for plane strain conditions.

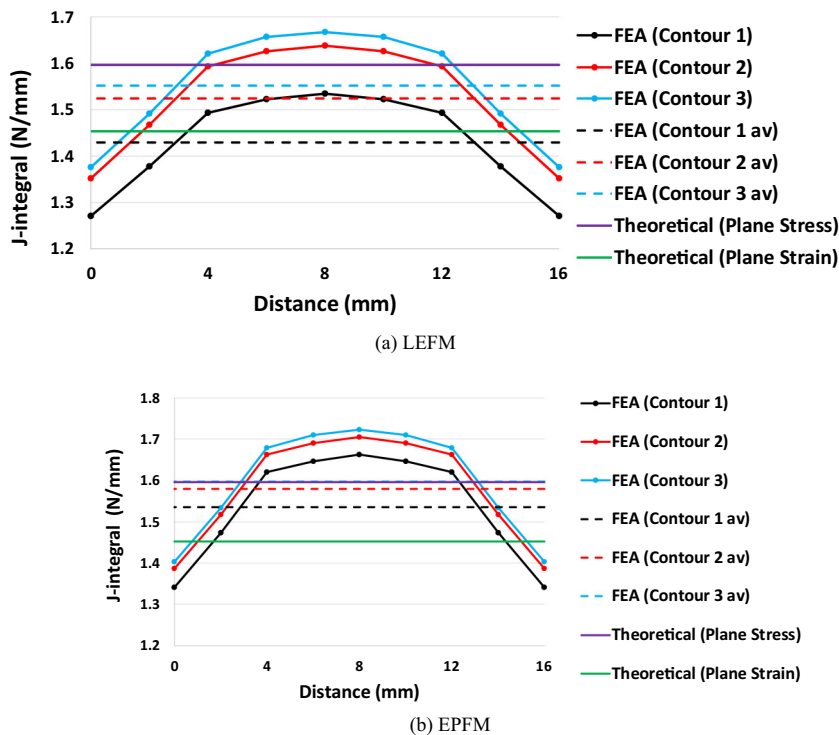


Fig. 6. J-integral distribution along thickness direction with P = 9kN and a = 20 mm.

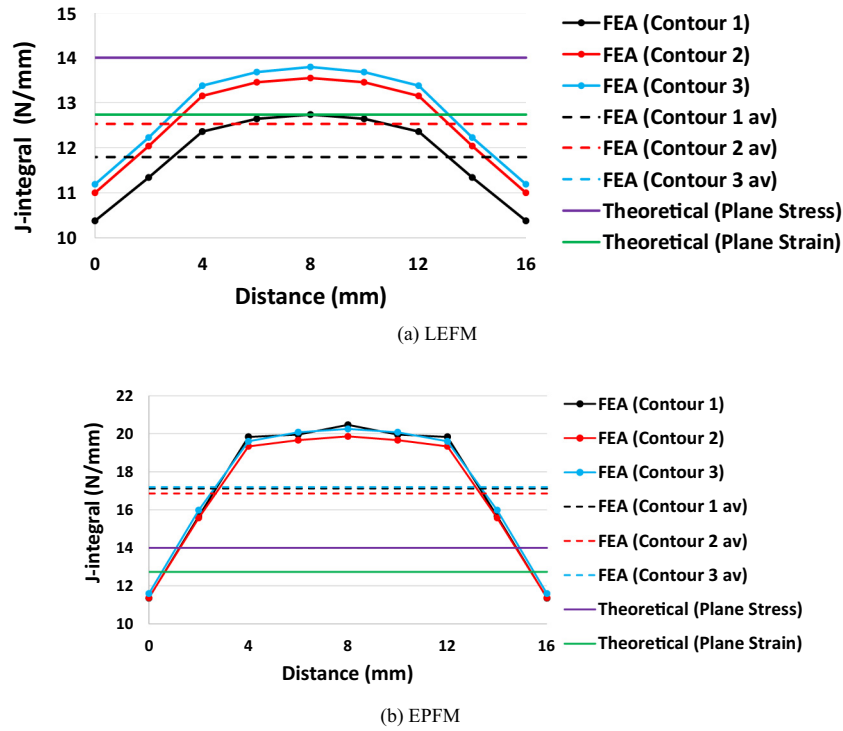


Fig. 7. J-integral distribution along thickness direction with $P = 9\text{ kN}$ and $a = 35\text{ mm}$.

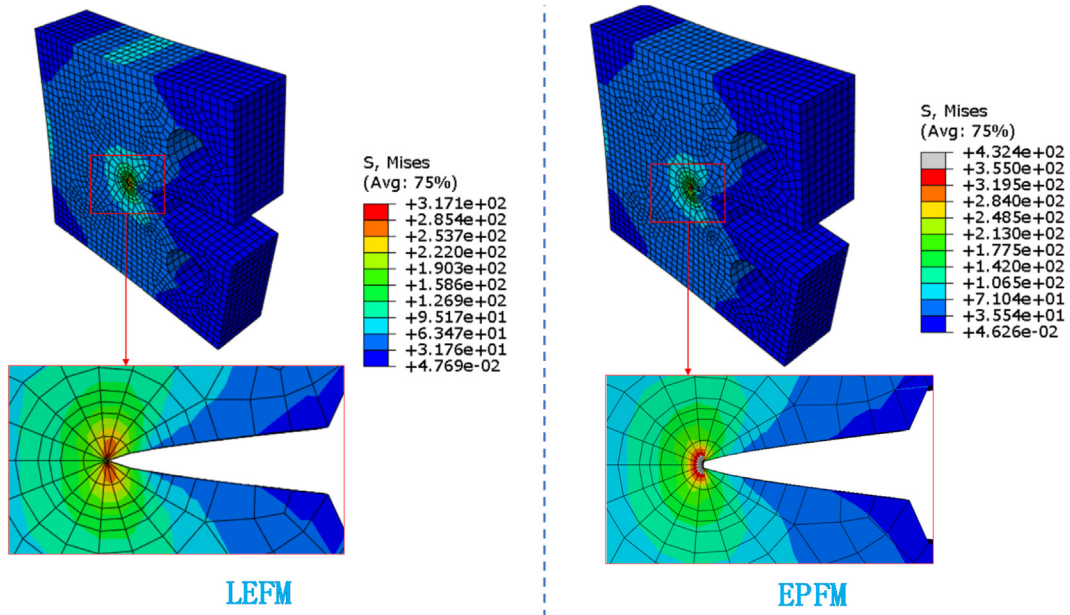


Fig. 8. Deformation comparison between LEFM and EPFM ($a = 20\text{ mm}$, $P = 9\text{ kN}$).

Table 5

Link between J-integral and SIF fitted using experimental results published in [3].

Load		Relationship
$P = 0.9\text{ kN}$	LEFM	$J = 4.56178 \times 10^{-8}K^2 - 1.51708 \times 10^{-6}K + 0.0005124$
	EPFM	$J = -3.37228 \times 10^{-18}K^5 + 2.13081 \times 10^{-14}K^4 - 5.14159 \times 10^{-11}K^3 + 1.08733 \times 10^{-7}K^2 - 3.72068 \times 10^{-5}K + 0.00822$
$P = 9.0\text{ kN}$	LEFM	$J = 4.56178 \times 10^{-6}K^2 - 1.51708 \times 10^{-4}K + 0.05124$
	EPFM	$J = 2.11949 \times 10^{-14}K^5 - 1.04526 \times 10^{-10}K^4 + 2.0334 \times 10^{-7}K^3 - 1.88665 \times 10^{-4}K^2 + 0.08964K - 16.23934$

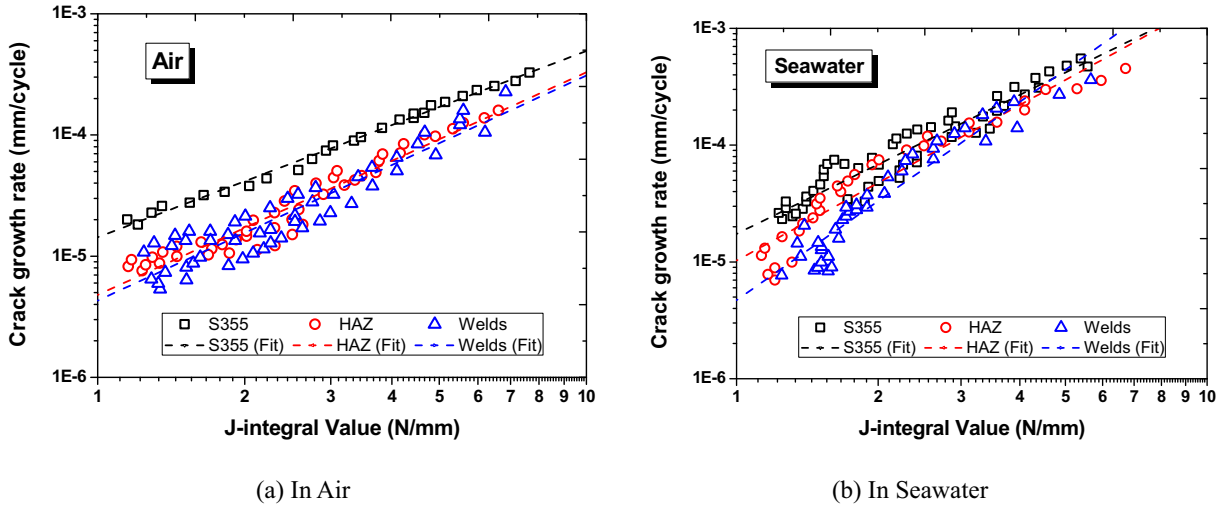


Fig. 9. Fatigue crack growth rate based on J-integrals (LEFM) in different environment.

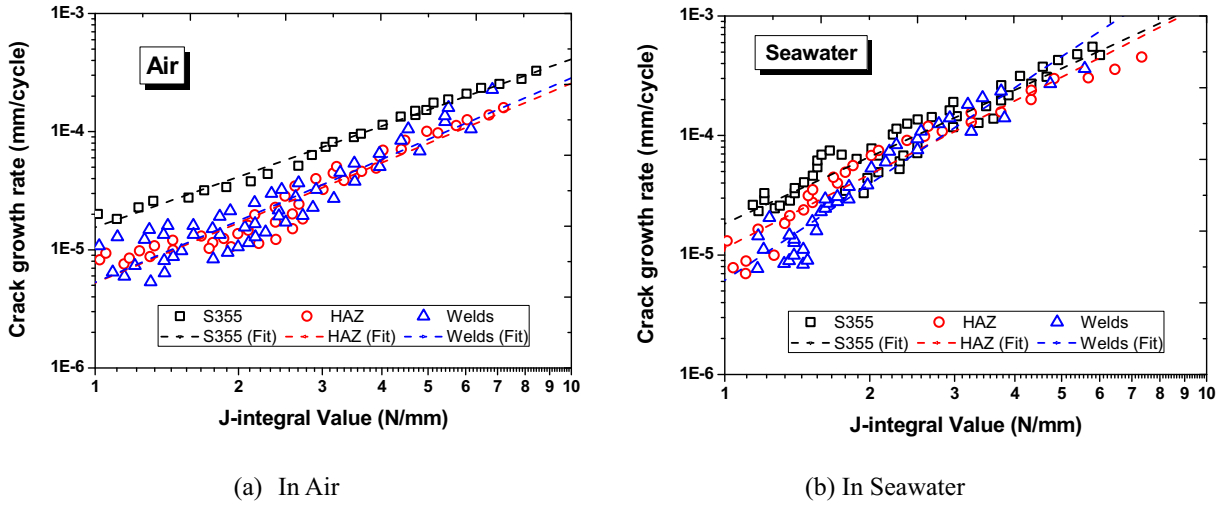


Fig. 10. Fatigue crack growth rate based on J-integrals (EPPM) in different environment.

To consider the plasticity around the crack tip, the fracture toughness SIFs could be replaced by J-integrals. The equation of J-based Paris law is presented in Eq. (6). The relationship between J-integrals and SIFs with different crack length are fitted, see using polynomial expression.

$$\frac{d\alpha}{dN} = C_J(\Delta J)^{m_j} \tag{6}$$

The fracture toughness SIFs of the parent material, HAZ, and welds in different environment reproduced from [3] are converted to J-integrals using the expressions listed in Table 5. The relationship between ΔJ and $d\alpha/dN$ are shown in Figs. 9 and 10. The relationship of ΔJ and $d\alpha/dN$ are fitted based on Eq. (5), and the fitted parameters of the “J-based Paris law” are summarized in Table 6. For LEFM, the exponent of J-integral based Paris law is one half of the exponent of SIF based Paris law in

Table 6
Parameters of fatigue crack propagation rate based on J-integrals.

	Environment	Material	P	R-ratio	C_J	m_j	R-square	$m_{K/2}$	$2^*m_j/m_K$
LEFM	Air	Steel (S355)	9.0	0.1	1.434×10^{-5}	1.538	0.99	1.541	1.00
		HAZ	9.0	0.1	4.798×10^{-6}	1.836	0.93	1.839	1.00
		Welds	9.0	0.1	4.305×10^{-6}	1.858	0.89	1.877	0.99
	Seawater	Steel (S355)	9.0	0.1	1.742×10^{-5}	1.977	0.91	1.980	1.00
		HAZ	9.0	0.1	1.025×10^{-5}	2.213	0.92	2.217	1.00
		Welds	9.0	0.1	4.682×10^{-6}	2.821	0.91	2.859	0.99
EPPM	Air	Steel (S355)	9.0	0.1	1.550×10^{-5}	1.423	0.99	1.541	0.92
		HAZ	9.0	0.1	5.238×10^{-6}	1.690	0.92	1.839	0.92
		Welds	9.0	0.1	5.314×10^{-6}	1.729	0.87	1.877	0.92
	Seawater	Steel (S355)	9.0	0.1	1.831×10^{-5}	1.857	0.91	1.980	0.94
		HAZ	9.0	0.1	1.146×10^{-5}	2.045	0.94	2.217	0.92
		Welds	9.0	0.1	6.146×10^{-6}	2.676	0.92	2.859	0.94

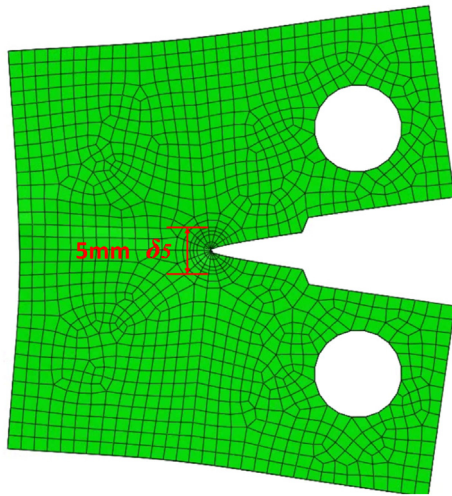


Fig. 11. Definition of CTOD for CT specimen.

terms of same material and environment. However, for EPFM, the exponent of J-integral based Paris law is less than one half of the exponent of SIF based Paris law in terms of same material and environment.

2.3. CTOD based fatigue crack propagation rate

The same finite element models used to calculate SIFs, see Fig. 2, are employed to calculate the CTOD according to LEFM and EPFM respectively. The crack opening displacement δ_s [39], which denotes relative displacement of the crack surfaces normal to the original undeformed crack plane over a gage length 5 mm, is used to capture the CTOD, see Fig. 11. The CTOD from FE simulation under according the principal of LEFM and EPFM are summarized in Table 7. The relationship between

CTOD and SIF with different crack length is fitted using polynomial expression, and the results are listed in Table 8.

To consider the plasticity around the crack tip, the fracture toughness SIFs could be converted to CTOD. The equation of “CTOD-based Paris law” is shown by Eq. (7). The fracture toughness SIF of the parent material, HAZ, and welds in different environments are taken from [3] and linked to CTOD derived parameters using the expressions listed in Table 8. The relationship between $\Delta\delta$ and $d\alpha/dN$ are shown in Figs. 12 and 13. The relationship of $\Delta\delta$ and $d\alpha/dN$ are fitted based on Eq. (7), and the fitted parameters of CTOD-based Paris law is summarized in Table 9. For LEFM, the exponent m of CTOD-based and SIF-based Paris law is almost identical for the same material and environment. However, the exponent m of CTOD-based Paris law (EPFM) is smaller than SIF-based value for the same material and environment.

$$\frac{d\alpha}{dN} = C_{\delta}(\Delta\delta)^{m_{\delta}} \tag{7}$$

2.4. CTOA based fatigue crack propagation rate

The same finite element models used to calculate SIFs, see Fig. 2, are used to calculate the CTOA according to LEFM and EPFM respectively. As is shown in Fig. 14, the crack tip opening angle is defined as the average angle of the two crack surfaces measured at a point 1 mm behind the crack tip [40,41]. The CTOA from FE simulation assuming LEFM and EPFM are summarized in Table 7. The relationship between CTOAs and SIFs are summarized in Table 10.

To consider the plasticity around the crack tip, the fracture toughness SIFs could also be converted to CTOA. The equation of “CTOA-based Paris law” is shown by Eq. (8). The fracture toughness SIF of the parent material, HAZ, and welds in different environment taken from [3] are linked to CTOA using the expressions listed in Table 10. The relationship between $\Delta\psi$ and $d\alpha/dN$ are shown in Figs. 15 and 16.

Table 7
Crack tip opening displacement and crack tip opening angle at P = 9.0 kN.

Crack length (mm)	LEFM (elastic part)		EPFM		Plastic part	
	CTOD (δ) ($\times 10^{-3}$ mm)	CTOA(δ) (Degrees)	CTOD (δ) ($\times 10^{-3}$ mm)	CTOA(δ) (Degrees)	CTOD (δ) ($\times 10^{-3}$ mm)	CTOA(δ) (Degrees)
a = 20	4.9503	0.4307	5.9357	0.5117	0.9854	0.081
a = 21	5.1889	0.4511	6.2611	0.5414	1.0722	0.0903
a = 22	5.4510	0.4744	6.6204	0.5730	1.1694	0.0986
a = 23	5.7453	0.4993	7.0238	0.6088	1.2785	0.1095
a = 24	6.0711	0.5290	7.4723	0.6468	1.4012	0.1178
a = 25	6.4348	0.5613	7.9742	0.6898	1.5394	0.1285
a = 26	6.8301	0.5943	8.5370	0.7391	1.7069	0.1448
a = 27	7.2903	0.6343	9.2177	0.7967	1.9274	0.1624
a = 28	7.7926	0.6801	10.0190	0.8643	2.2264	0.1842
a = 29	8.3838	0.7306	11.0322	0.9479	2.6484	0.2173
a = 30	9.0254	0.7883	12.2926	1.0507	3.2672	0.2624
a = 31	9.7697	0.8534	13.9064	1.1785	4.1367	0.3251
a = 32	10.6197	0.9287	15.9365	1.3388	5.3168	0.4101
a = 33	11.5908	1.0139	18.5810	1.5435	6.9902	0.5296
a = 34	12.7305	1.1173	22.5439	1.8507	9.8134	0.7334
a = 35	14.0296	1.2350	29.2597	2.4023	15.2301	1.1673

Table 8
Link between CTOD and SIF fitted using experimental results published in [3].

Load		Relationship
P = 0.9 kN	LEFM	$\delta = 8.33076 \times 10^{-7}K + 1.75204 \times 10^{-6}$
	EPFM	$\delta = 9.85854 \times 10^{-7}K - 1.68313 \times 10^{-5}$
P = 9.0 kN	LEFM	$\delta = - 3.10808 \times 10^{-11}K^2 + 8.39901 \times 10^{-6}K - 1.62376 \times 10^{-5}$
	EPFM	$\delta = 2.84971 \times 10^{-17}K^5 - 1.46997 \times 10^{-13}K^4 + 3.02335 \times 10^{-10}K^3 - 3.00138 \times 10^{-7}K^2 + 1.54223 \times 10^{-4}K - 0.02692$

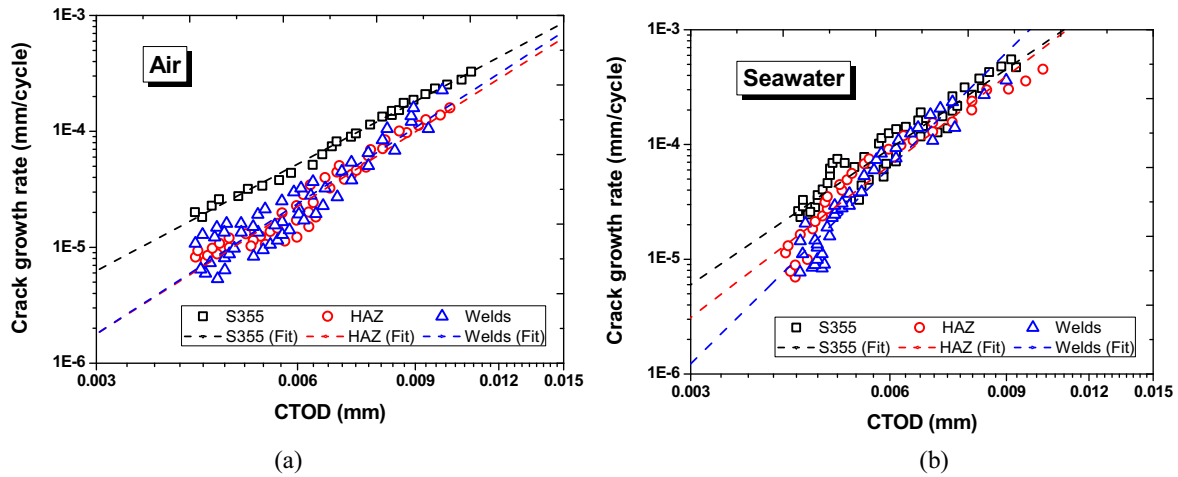


Fig. 12. Fatigue crack growth rate based on CTOD (LEFM) in different environment.

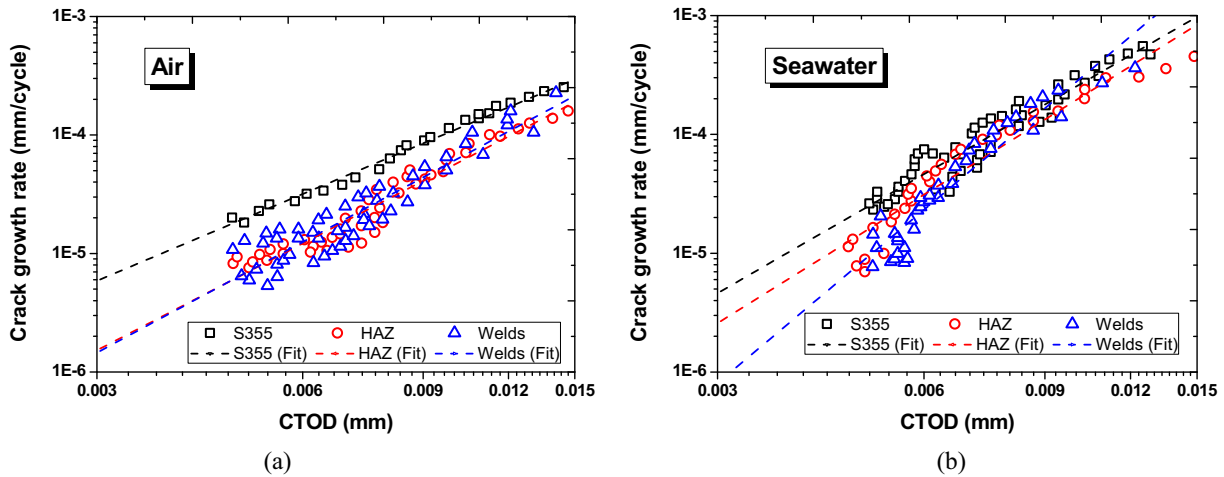


Fig. 13. Fatigue crack growth rate based on CTOD (EPFM) in different environment.

The relationship of $\Delta\psi$ and $d\alpha/dN$ are fitted based on Eq. (8), and fitted parameters of “CTOA-based Paris law” are summarized in Table 11. Interestingly, the exponent m of CTOD-based and CTOA-based Paris law is almost identical for the same materials and environments.

$$\frac{d\alpha}{dN} = C_{\psi}(\Delta\psi)^{m_{\psi}} \tag{8}$$

Table 9
Parameters of fatigue crack propagation rate based on CTOD.

	Environment	Material	P (kN)	R-ratio	C_6	m_6	R-square	m_6/m_K
LEFM	Air	Steel (S355)	9.0	0.1	335.5058	3.064	0.99	0.99
		HAZ	9.0	0.1	2992.2646	3.656	0.93	0.99
		Welds	9.0	0.1	4636.6039	3.731	0.88	0.99
	Seawater	Steel (S355)	9.0	0.1	51,380.6980	3.937	0.91	0.99
		HAZ	9.0	0.1	409,732.1098	4.407	0.92	0.99
		Welds	9.0	0.1	268,472,619.30	5.684	0.91	0.99
EPFM	Air	Steel (S355)	9.0	0.1	8.0705	2.433	0.99	0.79
		HAZ	9.0	0.1	55.8342	2.998	0.93	0.82
		Welds	9.0	0.1	97.6113	3.102	0.88	0.83
	Seawater	Steel (S355)	9.0	0.1	1152.1261	3.329	0.91	0.84
		HAZ	9.0	0.1	3016.4769	3.594	0.92	0.81
		Welds	9.0	0.1	1,377,843.843	4.848	0.91	0.85

3. Residual stress simulation

3.1. Material properties and welding procedures

Modelling of the welding procedure is carried out using commercially available FEA software, ABAQUS [31]. A sequentially coupled thermo-mechanical analysis is performed, where the temperature field was introduced as a predefined field in the mechanical analysis.

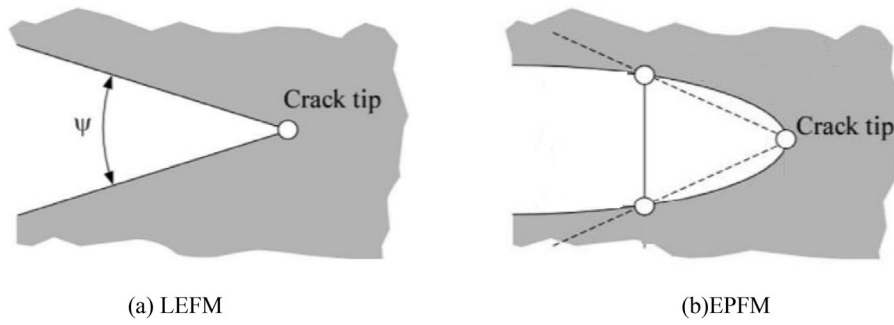


Fig. 14. Definition of CTOA for CT specimen [40].

Table 10

Link between CTOA and SIF fitted using experimental results published in [3].

Load		Relationship
P = 0.9 kN	LEFM	$\psi = -2.12541 \times 10^{-12}K^3 - 4.46496 \times 10^{-9}K^2 + 5.99787 \times 10^{-5}K + 0.00496$
	EPFM	$\psi = 2.53981 \times 10^{-12}K^3 - 2.36807 \times 10^{-8}K^2 + 8.605 \times 10^{-5}K + 1.68894 \times 10^{-5}$
P = 9.0 kN	LEFM	$\psi = 1.05843 \times 10^{-8}K^2 + 7.12846 \times 10^{-4}K + 0.0047$
	EPFM	$\psi = 2.86819 \times 10^{-15}K^5 - 1.4712 \times 10^{-11}K^4 + 2.99201 \times 10^{-8}K^3 - 2.94958 \times 10^{-5}K^2 + 0.01501K - 2.6467$

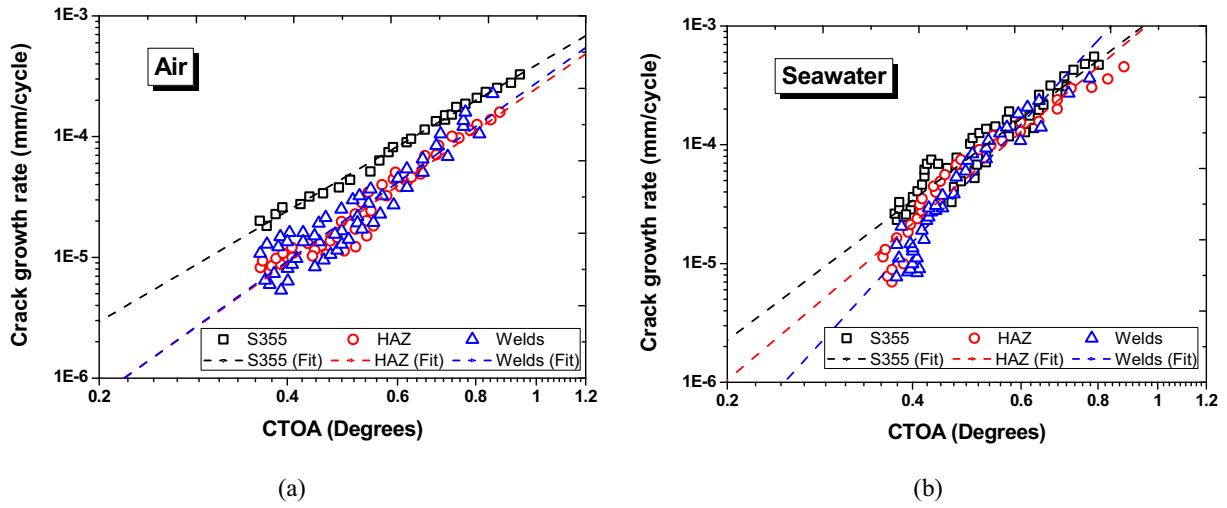


Fig. 15. Fatigue crack growth rate based on CTOA (LEFM) in different environment.

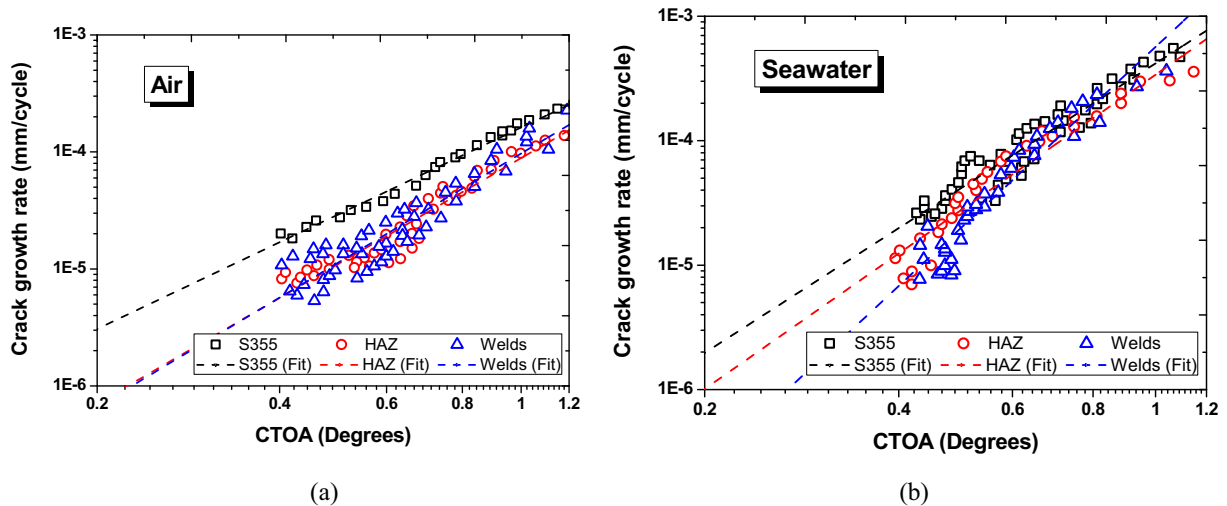


Fig. 16. Fatigue crack growth rate based on CTOA (EPFM) in different environment.

Table 11
Parameters of fatigue crack propagation rate based on CTOA.

	Environment	Material	P	R-ratio	C_{ψ}	m_{ψ}	R-square	m_{ψ}/m_{δ}
LEFM	Air	Steel (S355)	9.0	0.1	3.926×10^{-4}	3.043	0.92	0.99
		HAZ	9.0	0.1	2.499×10^{-4}	3.634	0.93	0.99
		Welds	9.0	0.1	2.775×10^{-4}	3.709	0.88	0.99
	Seawater	Steel (S355)	9.0	0.1	1.229×10^{-3}	3.914	0.91	0.99
		HAZ	9.0	0.1	1.201×10^{-3}	4.380	0.92	0.99
		Welds	9.0	0.1	2.671×10^{-3}	5.652	0.91	0.99
EPFM	Air	Steel (S355)	9.0	0.1	1.618×10^{-4}	2.465	0.99	1.01
		HAZ	9.0	0.1	8.865×10^{-5}	3.003	0.93	1.00
		Welds	9.0	0.1	9.705×10^{-5}	3.096	0.88	1.00
	Seawater	Steel (S355)	9.0	0.1	4.174×10^{-4}	3.326	0.91	1.00
		HAZ	9.0	0.1	3.421×10^{-4}	3.612	0.93	1.01
		Welds	9.0	0.1	5.671×10^{-4}	4.827	0.91	1.00

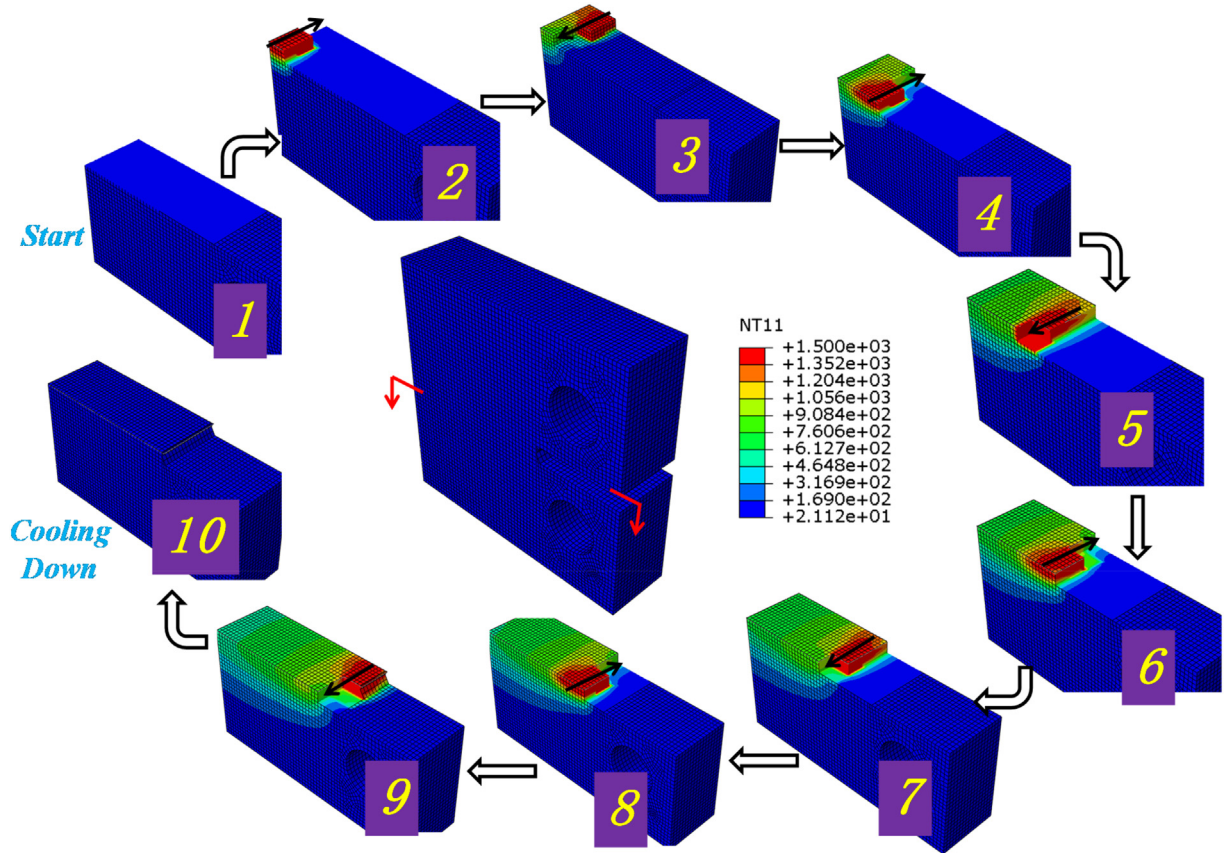


Fig. 17. Predicted temperature distribution during the welding process (Unit: °C).

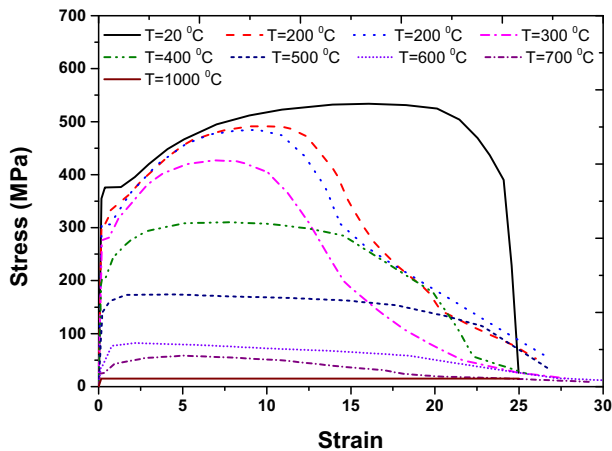


Fig. 18. Temperature-dependent stress-strain relationship of S355 Steel.

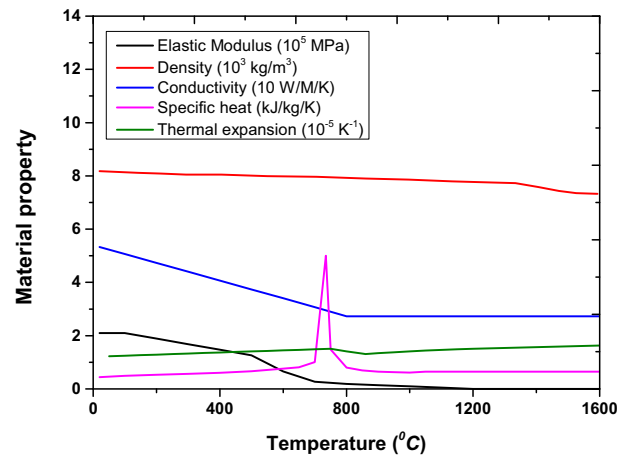
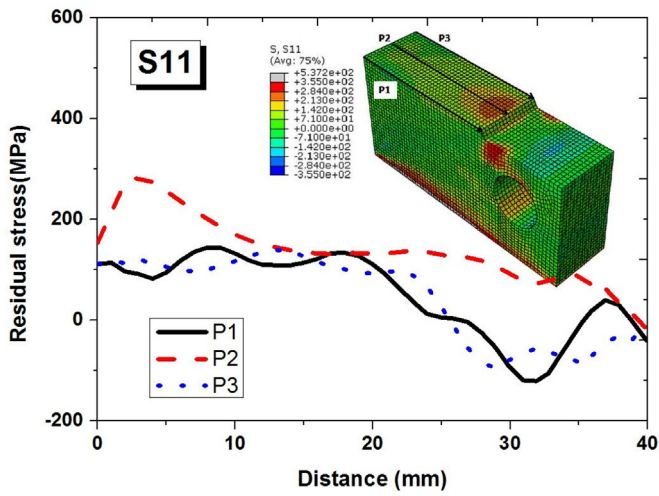


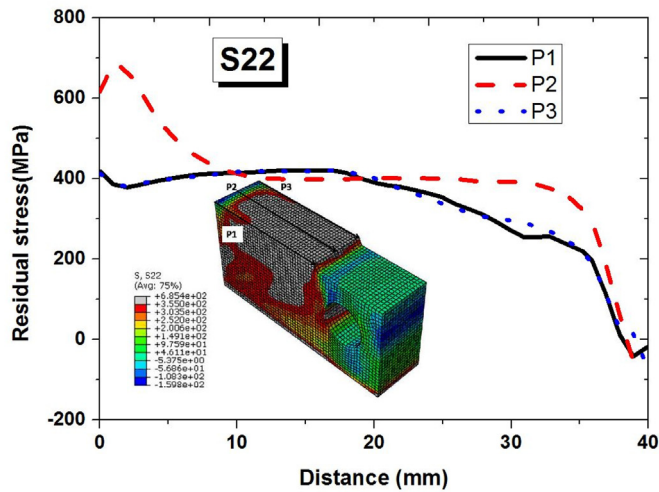
Fig. 19. Thermal and mechanical properties of steel S355 versus temperature.

Fig. 17 shows the temperature state for the assumed welding process, including the initial status, from the first pass to the eighth pass, and at the final state, cooled to the room temperature. The assumed thickness of welds is 4mm.

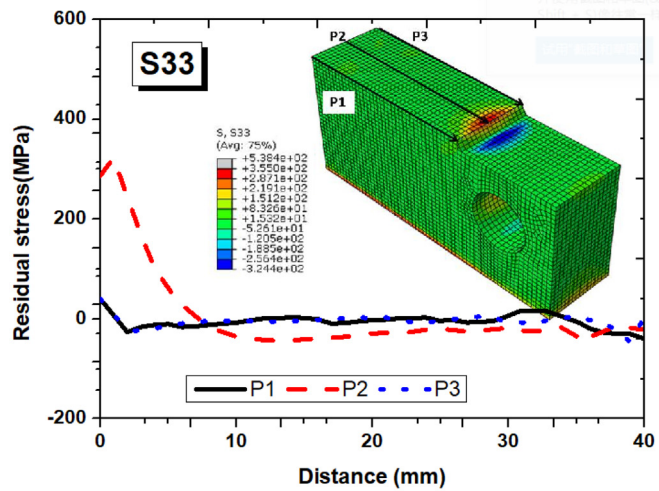
The stress-strain relationship of steel S355 used in FEA is shown in Fig. 18. This diagram is based on material tests on elevated temperature reported in [42]. Additional thermal properties used in the FEA are shown in Fig. 19 according to EN 1993-1-2 [43]. The annealing



(a)

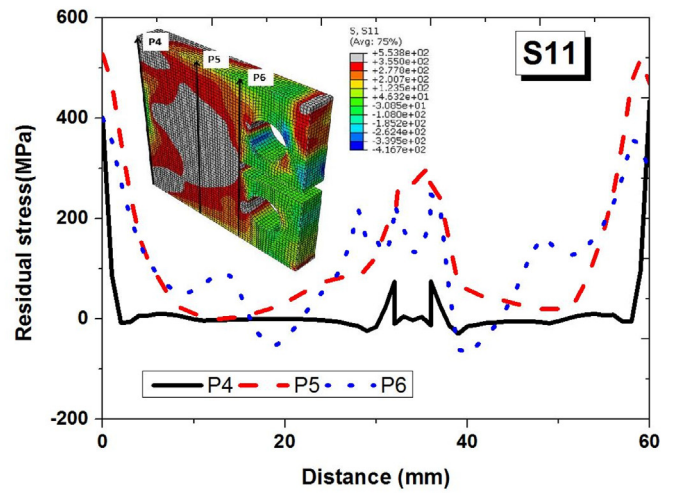


(b)

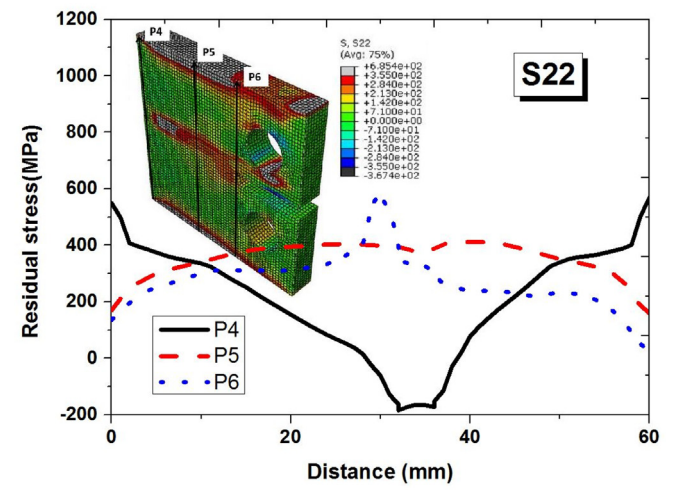


(c)

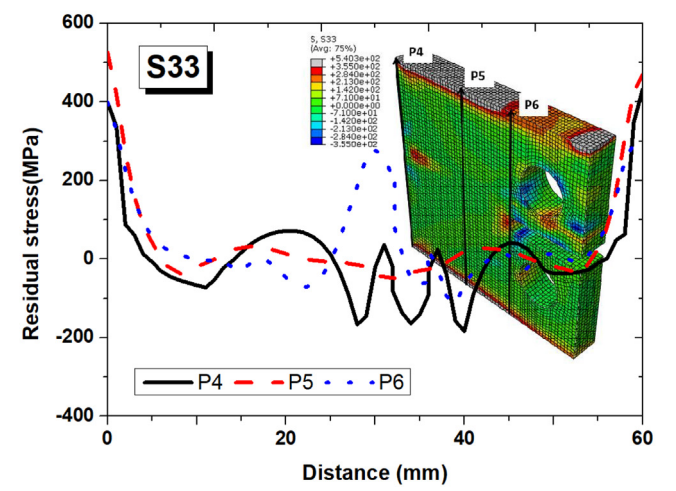
Fig. 20. Residual stress distribution along the transverse direction.



(a)



(b)



(c)

Fig. 21. Residual stress distribution along the loading direction.

Table 12
Residual stress effects on J-integrals based on LEFM.

Crack length (mm)	Contour-3-av (N/mm)		Contour-3-Max (N/mm)		Contour-3-Min (N/mm)		Max/Min		$\Delta J_{res}/\Delta J$
	P = 9 kN	P = 0.9 kN	P = 9 kN	P = 0.9 kN	P = 9 kN	P = 0.9 kN	P = 9 kN	P = 0.9 kN	
a = 20	1.50	0.10	2.46	0.67	0.23	-0.18	10.70	-3.72	1.00
a = 21	2.43	0.30	4.21	1.04	0.25	-0.29	16.84	-3.59	1.38
a = 22	2.56	0.35	4.48	1.04	0.41	-0.26	10.93	-4.00	1.30
a = 23	2.57	0.29	4.51	0.87	0.72	-0.26	6.26	-3.35	1.20
a = 24	2.77	0.29	4.67	0.80	0.79	-0.08	5.91	-10.00	1.17
a = 25	3.09	0.26	4.86	0.73	1.00	-0.20	4.86	-3.65	1.19
a = 26	3.44	0.23	5.15	0.63	1.29	-0.13	3.99	-4.85	1.19
a = 27	3.63	0.19	5.59	0.53	1.53	-0.06	3.65	-8.83	1.12
a = 28	3.83	0.15	6.00	0.47	1.86	-0.19	3.23	-2.47	1.05
a = 29	4.28	0.13	6.51	0.38	2.20	-0.10	2.96	-3.80	1.03
a = 30	4.98	0.11	7.09	0.30	2.62	-0.12	2.71	-2.50	1.04
a = 31	5.84	0.11	8.07	0.31	3.20	-0.06	2.52	-5.17	1.04
a = 32	6.76	0.13	9.43	0.33	3.95	-0.01	2.39	-33.00	1.02
a = 33	7.82	0.11	10.90	0.25	4.99	-0.07	2.18	-3.57	0.99
a = 34	9.44	0.12	12.78	0.24	6.21	-0.07	2.06	-3.43	0.99
a = 35	13.25	0.14	16.23	0.32	8.88	-0.11	1.83	-2.91	1.14

Table 13
Link between J-integrals and SIFs including the influence of residual stresses.

Load	Relationship
P = 0.9 kN	$J = 1.48934 \times 10^{-9} K^5 - 8.77761 \times 10^{-7} K^4 + 2.01592 \times 10^{-4} K^3 - 2.246 \times 10^{-2} K^2 + 1.207K - 24.69793$
P = 9.0 kN	$J = 7.83522 \times 10^{-14} K^5 - 4.33489 \times 10^{-10} K^4 + 9.39064 \times 10^{-7} K^3 - 9.89377 \times 10^{-4} K^2 + 0.51121K - 101.44954$

temperature is assumed 1000 °C meaning that the plastic strains are zero when the temperature is above it, to consider the phase transition effect. The low end of the temperature range and the high end of the temperature range within which the phase change occurs is assumed as 1450 °C and 1500 °C respectively. The latent heat is assumed to be 247 J/g for consideration of released and absorbed thermal energy during the first-order phase transition.

The welding torch is modelled with a heat boundary 1500 °C between the current welding fusion zone and the neighboring zone. The current fusion elements are activated with a prescribed temperature of 1500 °C in the whole model after the welding torch passed the current fusion zone simulated by the steady heat transfer with defined pass time. Convection and radiation are considered by applying the surface film contact with a coefficient 15 W/(m²K) and surface radiation

contact with the emissivity 0.9. The top and bottom surface is fixed in the mechanical model.

3.2. Residual stress

Fig. 20 shows the ratio of residual stress distribution in the x-direction, coordinate axes are shown in Fig. 3. The residual stress component S11 along the x-direction is in compression from 0mm to 20mm and in tension from 20mm to 40mm. The residual stress component S22 along the x-direction is in tension, mostly beyond the yielding stress. The residual stress component S33 is relatively very small except local stresses close to the notch. Fig. 21 presented residual stress distribution along the loading direction. The residual stress component S11 in the central part (from 5 mm to 55 mm length) is relatively smaller than

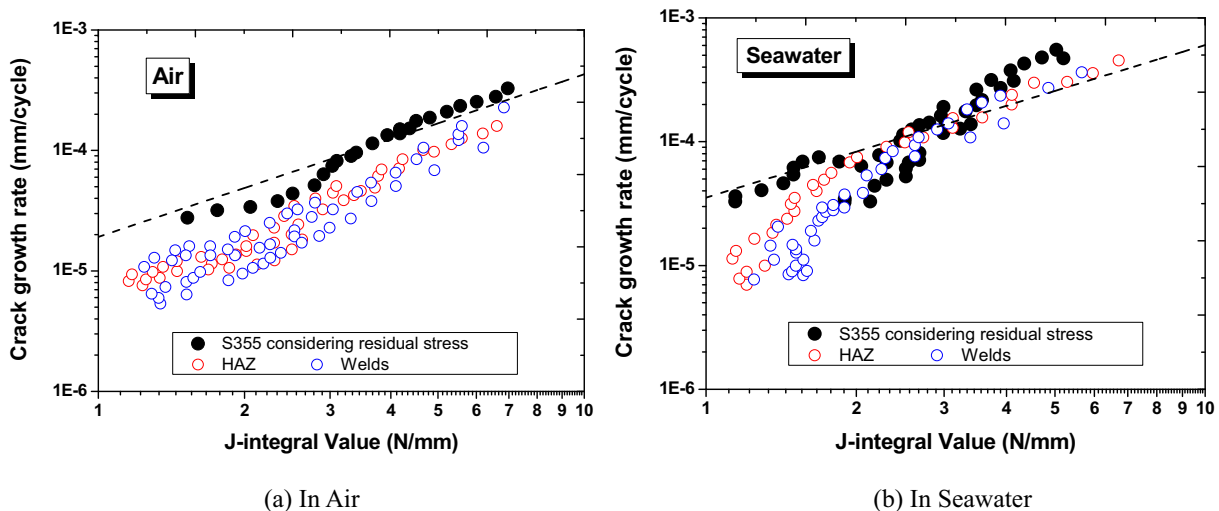


Fig. 22. J-integral (LEFM) based fatigue crack growth rate comparisons in different environment.

Table 14
Residual stress effects on J-integrals based on EPFM.

Crack length (mm)	Contour-3-av (N/mm)		Contour-3-Max (N/mm)		Contour-3-Min (N/mm)		Max/Min	
	P = 9 kN	P = 0.9 kN	P = 9 kN	P = 0.9 kN	P = 9 kN	P = 0.9 kN	P = 9 kN	P = 0.9 kN
a = 20	3.15	0 (-0.0787)	5.07	0.5120	0.59	-0.4950	8.59	-1.03
a = 21	3.57	0.0580	6.14	0.5450	1.06	-0.3630	5.79	-1.50
a = 22	3.68	0.0959	6.22	0.3679	1.36	-0.3189	4.57	-1.15
a = 23	3.58	0.0334	5.77	0.3332	1.40	-0.2973	4.12	-1.12
a = 24	3.73	0.0021	5.63	0.4424	1.33	-0.3015	4.23	-1.47
a = 25	4.09	0 (-0.0237)	5.87	0.4426	1.52	-0.4110	3.86	-1.08
a = 26	4.53	0(-0.0007)	6.70	0.3427	1.84	-0.4533	3.64	-0.76
a = 27	4.79	0(-0.0052)	7.58	0.2881	2.24	-0.5107	3.38	-0.56
a = 28	5.13	0(-0.0605)	7.90	0.2002	2.51	-0.6002	3.15	-0.33
a = 29	5.81	0(-0.1130)	8.43	0.2983	2.79	-0.5055	3.02	-0.59
a = 30	6.97	0(-0.1092)	9.44	0.3783	3.42	-0.5937	2.76	-0.64
a = 31	8.56	0(-0.0110)	11.71	0.4467	4.58	-0.5429	2.56	-0.82
a = 32	10.46	0(-0.0402)	14.53	0.4509	6.40	-0.6610	2.27	-0.68
a = 33	13.04	0(-0.0936)	17.58	0.3657	8.09	-0.7124	2.17	-0.51
a = 34	17.81	0(-0.1104)	23.04	0.3732	10.91	-0.6754	2.11	-0.55
a = 35	26.84	0(-0.0815)	34.52	0.5120	15.38	-0.4950	2.24	-1.03

at the outer part (from 0 mm to 5 mm and from 55 mm to 60 mm). The residual stress components S22 of the "Path 4" and "Path 6" are opposite, and the residual stress component S22 of Path 5 is mostly beyond the yielding stress. The residual stress component S33 is relatively very small except for local stress close to the ends, near the notch and at the far-away ends.

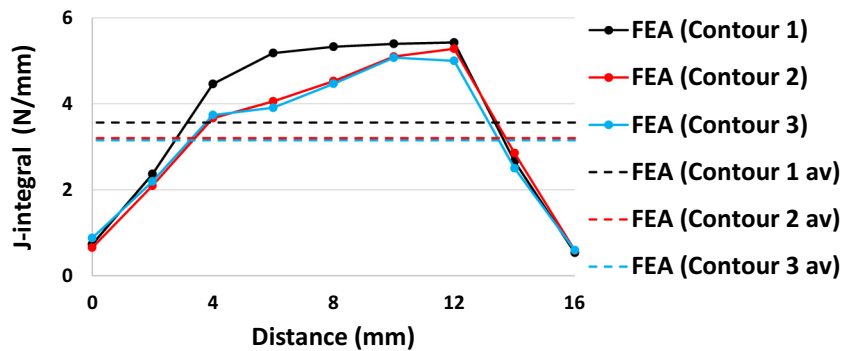
4. Residual stress effects on fatigue crack propagation rate

The residual stresses components obtained from FEA by modelling welding process in Section 3 are introduced into the fracture

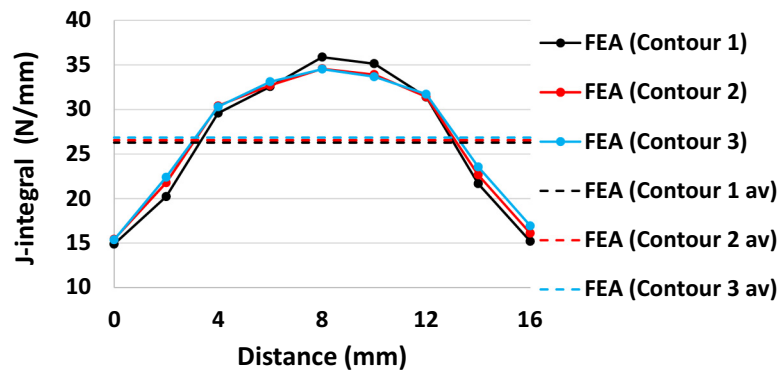
parameters FE models with different crack lengths using mesh-to-mesh solution mapping [31], because the mesh size of welding model in Section 3 is different from the model to obtain the fracture parameters.

4.1. LEFM-based fatigue crack propagation rate

Finite element models, as shown in Fig. 2, are also used to calculate J-integrals (LEFM) by importing the residual stress as the predefined stresses. The J-integrals (LEFM) based on FE simulation considering residual stress effects is summarized in Table 12. The relationship using



(a) a = 21 mm



(b) a = 35 mm

Fig. 23. J-integral distribution along thickness direction after considering residual stress.

Table 15
List of expressions between J-integrals and SIFs after considering residual stress.

Load	Relationship
$P = 0.9 \text{ kN}$	$J = 1.49443 \times 10^{-4} K^3 - 0.0312 K^2 + 2.15849 K - 49.43234 \quad K < 77.14 / J = 0 \quad K > 77.14$
$P = 9.0 \text{ kN}$	$J = 6.04443 \times 10^{-14} K^5 - 3.15731 \times 10^{-10} K^4 + 6.5324 \times 10^{-7} K^3 - 6.52137 \times 10^{-4} K^2 + 0.31729 K - 57.1885$

polynomial expression between J-integrals (LEFM) and SIF with different crack length is listed in Table 13. The fracture toughness SIFs of steel in different environment reproduced from [3] are converted to J-integrals (LEFM) using the expressions listed in Table 13. As shown in Fig. 22, fatigue crack propagation rate based on parent material considering the residual stress is compared to weld material and HAZ in terms of J-integrals (LEFM). The predicted fatigue crack propagation rate combining the parent materials with residual stress does not agree well with properties of welds and HAZ based on J-integrals (LEFM).

4.2. EPFM based fatigue crack propagation rate

The J-integrals (EPFM) based on FE simulation considering residual stress effects is shown in Table 14. The J-integral distribution in the thickness direction including effect of residual stresses is shown in Fig. 23. The J-integral distribution is not symmetric after the residual stresses are introduced. The ratio between maximum and minimum J-integral increased compared to the residual stress-free situation. The relationship using polynomial expression between J-integrals (EPFM) and SIF with different crack length is listed in Table 15. As shown in Fig. 24, the fatigue crack propagation rate based on the parent material considering the residual stress is compared with test results of welds and HAZ of J-integrals according to EPFM. The predicted fatigue crack propagation rate assuming the parent material with residual stress agreed well with experimental results of welds and HAZ in air, but there is a relatively larger difference in seawater environment in terms of J-integrals (EPFM).

4.3. CTOD-based fatigue crack propagation rate

The CTOD (EPFM) values obtained by FE simulation considering residual stress effects is summarized in Table 16. The relationship using polynomial expression between CTOD (EPFM) and SIFs with different crack length is shown in Table 17. As shown in Fig. 25, fatigue crack propagation rate assuming the parent material and considering the residual stress is compared to weld material and HAZ in terms of CTOD (EPFM). The predicted fatigue crack propagation rate combining the

Table 16
Crack tip opening displacement and crack tip opening angle including the influence of residual stresses.

Crack length (mm)	CTOD (δ) ($\times 10^{-3} \text{ mm}$)		CTOA(δ) (degrees)	
	$P = 9 \text{ kN}$	$P = 0.9 \text{ kN}$	$P = 9 \text{ kN}$	$P = 0.9 \text{ kN}$
a = 20	6.14	0.57	0.57	0.045
a = 21	6.74	0.60	0.58	0.047
a = 22	7.02	0.64	0.61	0.050
a = 23	7.29	0.63	0.64	0.052
a = 24	7.59	0.58	0.67	0.051
a = 25	7.81	0.72	0.70	0.052
a = 26	7.93	0.78	0.72	0.057
a = 27	8.47	0.81	0.77	0.059
a = 28	9.58	0.87	0.86	0.060
a = 29	10.98	0.83	0.95	0.058
a = 30	12.48	0.96	1.08	0.065

parent materials with residual stress agreed well with experimental results of welds and HAZ in terms of CTOD (EPFM).

4.4. CTOA-based fatigue crack propagation rate

The CTOA (EPFM) values obtained by FE simulation considering residual stress effects are summarized in Table 16. The relationship using polynomial expression between CTOA (EPFM) and SIFs with different crack length is listed in Table 18. As shown in Fig. 26, fatigue crack propagation rate assuming the parent material and considering the residual stress is compared with test results of welds and HAZ in terms of CTOA (EPFM). The predicted fatigue crack propagation rate combining the parent materials with residual stress agreed well with experimental results of welds and HAZ in terms of CTOA (EPFM).

4.5. Discussions

Table 19 provides the fatigue crack growth rate parameters comparing different environment. Compared with the parent steel,

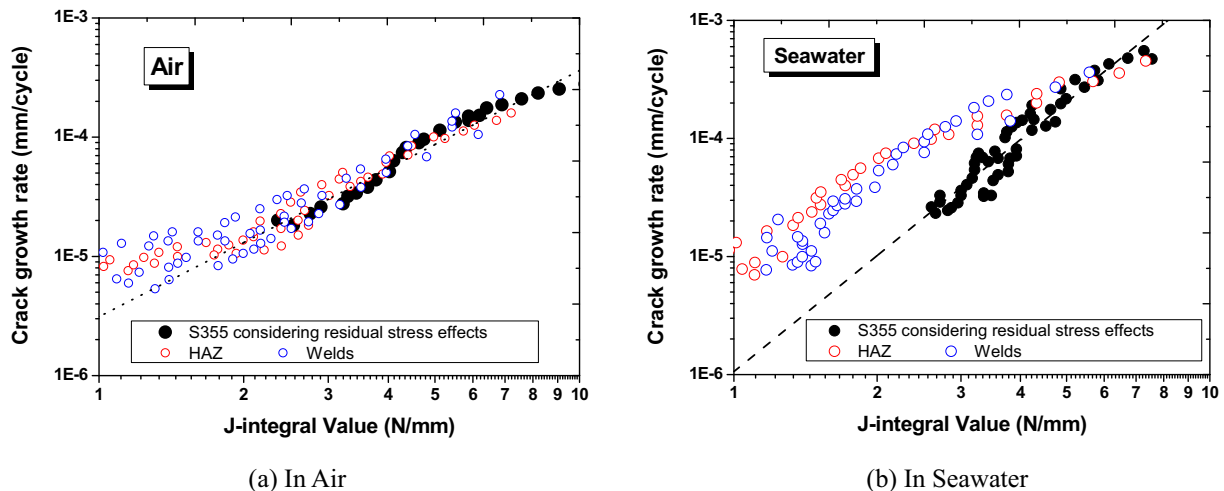


Fig. 24. J-integral based fatigue crack growth rate comparisons in different environment.

Table 17

Links between CTOD and SIFs including the influence of residual stresses.

Load	Relationship
$P = 0.9 \text{ kN}$	$\delta = 2.41643 \times 10^{-13} K^5 - 1.40688 \times 10^{-10} K^4 + 3.14855 \times 10^{-8} K^3 - 3.34936 \times 10^{-6} K^2 + 1.76825 \times 10^{-4} K - 0.00314$
$P = 9.0 \text{ kN}$	$\delta = 7.20855 \times 10^{-17} K^5 - 3.67323 \times 10^{-13} K^4 + 7.35676 \times 10^{-10} K^3 - 7.07481 \times 10^{-7} K^2 + 3.33711 \times 10^{-4} K - 0.05597$

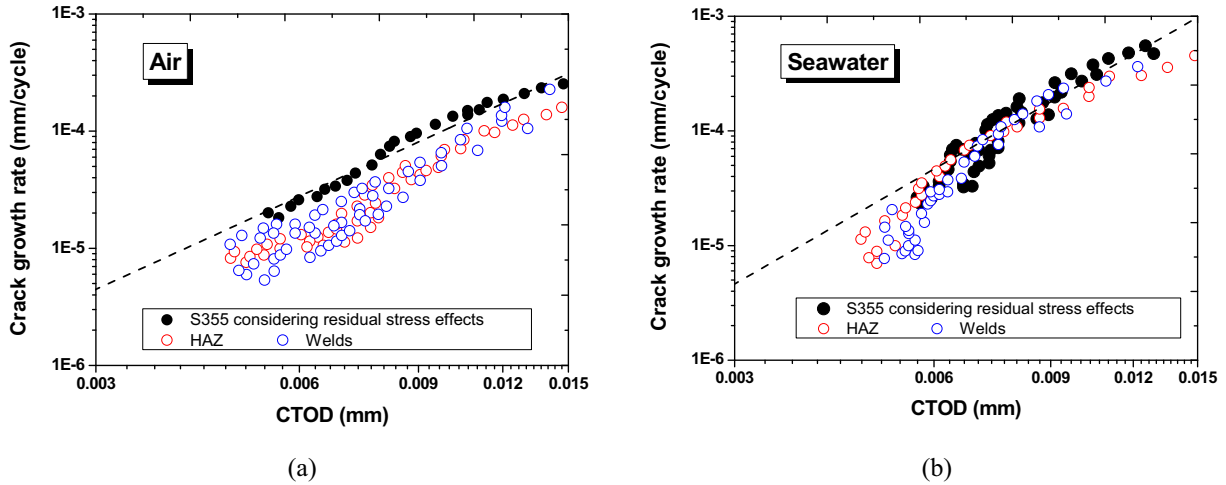


Fig. 25. CTOD-based fatigue crack growth rate comparisons in different environment.

the exponent of fatigue crack growth rate m of the parent material including the residual stress is generally increased based on J-integrals (LEFM), J-integrals (EPFM), CTOD (EPFM) and CTOA (EPFM) models. This trend agrees well with experimental results [3]. The exponent of fatigue crack growth rate based on LEFM calculation tends to be smaller than obtained in experiments results [3]. The exponent of fatigue

crack growth rate based on EPFM tends to be closer to experimental results [3]. The fatigue crack growth rate parameters based on the parent material, including the residual stress, could be used as a surrogate method in the prediction models using CTOD- and CTOA- based Paris law (EPFM) in case that fatigue experiments are unavailable due to cost and time limitation, as shown in Figs. 25 and 26.

Table 18

List of expressions between CTOA and SIFs after considering residual stress.

Load	Relationship
$P = 0.9 \text{ kN}$	$\psi = 2.49568 \times 10^{-11} K^5 - 1.50729 \times 10^{-8} K^4 + 3.53792 \times 10^{-6} K^3 - 4.01524 \times 10^{-4} K^2 + 0.02231K - 0.43615$
$P = 9.0 \text{ kN}$	$\psi = 3.47618 \times 10^{-15} K^5 - 1.68408 \times 10^{-11} K^4 + 3.26409 \times 10^{-8} K^3 - 3.03197 \times 10^{-5} K^2 + 0.01409K - 2.10158$

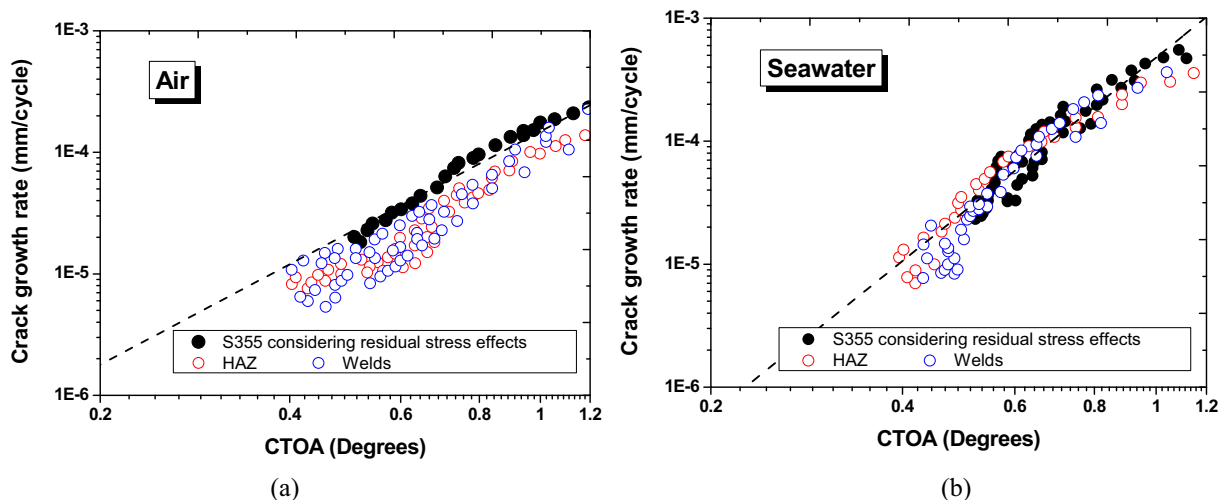


Fig. 26. CTOA-based fatigue crack growth rate comparisons in different environment.

Table 19
Summary of fatigue crack growth rate parameters in different environments.

Items			Experimental results		FEA assuming on the parent material with (without) residual stress	
			C	m	C	m
Air	J (LEFM)	HAZ	4.798×10^{-6}	1.836	1.914×10^{-5}	1.35
		Welds	4.305×10^{-6}	1.858	(1.434×10^{-5})	(1.538)
	J (EPFM)	HAZ	5.238×10^{-6}	1.690	3.535×10^{-5}	1.897
		Welds	5.314×10^{-6}	1.729	(1.804×10^{-5})	(1.541)
	CTOD (EPFM)	HAZ	55.8342	2.998	19.9756	2.636
		Welds	97.6113	3.102	(8.0705)	(2.433)
CTOA (EPFM)	HAZ	8.865×10^{-5}	3.003	1.4839×10^{-4}	2.744	
	Welds	9.705×10^{-5}	3.096	(1.6180×10^{-4})	(2.465)	
Seawater	J (LEFM)	HAZ	1.025×10^{-5}	2.213	3.181×10^{-5}	2.057
		Welds	4.682×10^{-6}	2.821	(1.742×10^{-5})	(1.977)
	J (EPFM)	HAZ	1.146×10^{-5}	2.045	1.0595×10^{-6}	3.263
		Welds	6.146×10^{-6}	2.676	(1.831×10^{-5})	(1.980)
	CTOD (EPFM)	HAZ	3016.4769	3.594	30,067.7	4.018
		Welds	1,377,843.843	4.848	(1152.1261)	(3.329)
	CTOA (EPFM)	HAZ	3.421×10^{-4}	3.612	4.7918×10^{-4}	4.154
		Welds	5.671×10^{-4}	4.827	(4.174×10^{-4})	(3.326)

Note: the value in the bracket is for steel without considering residual stress.

5. Conclusions

The parameters of corrosion fatigue crack growth rate for Q355J2 steel are calculated using "Paris' law" fatigue parameters, m and C , evaluated using stress intensity factor (SIF), J-integral, crack tip opening displacement (CTOD) and crack tip opening angle (CTOA) approach. The residual stresses effect on the corrosion fatigue crack growth rate is investigated by considering the numerically predicted residual stress distribution due to welding process. The corrosion fatigue crack growth rate assuming the parent material and considering residual stress is compared to the rates obtained for the weld material and heat affected zone (HAZ) material. The following conclusion are obtained:

- (1) For LEFM, the exponent m of the "J-integral based Paris law" is almost one half of the exponent m of the "SIF based Paris law" parameters for the same materials and environments. However, for EPFM, the exponent m of "J-integral based Paris law" is less than one half of the exponent of "SIF based Paris law" for the same material and environment.
- (2) For LEFM, the exponent m of "CTOD-based" and "SIF-based Paris law" is almost identical to the same material and environment. However, the exponent m of "CTOD-based Paris law" (EPFM) is smaller than "SIF-based" m for the same materials and environments. The exponent m of "CTOD-based" and "CTOA-based Paris law" is almost identical for the same materials and environments.
- (3) The predicted fatigue crack propagation rate based on the parent materials with residual stress did not agree well with values obtained from experiments on welds and HAZ when J-integrals (LEFM) is used. The predicted fatigue crack propagation rate based on the parent material with residual stress agrees well with experimental results of welds and HAZ in air, but has a relatively larger difference in seawater environment based on J-integrals (EPFM). When unloading occurs in an elastic-plastic material, the J integral with the assumption of nonlinear elastic material to characterize fatigue crack growth rate needed to be further investigated.
- (4) The predicted fatigue crack propagation rate assuming the parent materials with residual stress agreed well with experimental results of welds and HAZ when CTOD and CTOA (EPFM) approach is used. The fatigue crack growth rate parameters based on the parent material including the residual stress could be used as a surrogate method in the prediction models using CTOD- and

CTOA- based Paris law (EPFM) in case that fatigue experiments are unavailable due to cost and time limitation.

- (5) The exponent m of the fatigue crack growth rate of parent material including residual stress generally is larger when J-integrals (LEFM), J-integrals (EPFM), CTOD (EPFM) and CTOA (EPFM) approaches are used. This trend is consistent with experimental results in the literature. The exponent m of fatigue crack growth rate based on LEFM calculation tends to be smaller than obtained from experiments results. The exponent m of fatigue crack growth rate based on EPFM tends to be closer to the experimental results. This indicates possibility to predict the fatigue crack growth rate parameters based on the parent material and residual stress in case that fatigue experiments are unavailable due to cost and time limitation.
- (6) To effectively evaluate the fatigue crack growth rate of complicated geometry welded steel structures, the surrogate method based only on parent material introducing residual stress, the residual stress effects on the threshold (Stage I and Stage III of Paris law) of fatigue crack propagation needs to be studied further.

Data availability statement

The data will be made available upon request.

CRediT authorship contribution statement

Haohui Xin: Investigation, Formal analysis, Writing - original draft.
Milan Veljkovic: Writing - review.

Declaration of competing interest

The authors declare that they have no known competing financial interests or personal relationships that could have appeared to influence the work reported in this paper.

References

- [1] L. Arany, S. Bhattacharya, J. Macdonald, S.J. Hogan, Design of monopiles for offshore wind turbines in 10 steps, *Soil Dyn. Earthq. Eng.* 92 (2017) 126–152.
- [2] A. Mehmanparast, F. Brennan, I. Tavares, Fatigue crack growth rates for offshore wind monopile weldments in air and seawater: SLIC inter-laboratory test results, *Mater. Des.* 114 (2017) 494–504.
- [3] O. Adedipe, F. Brennan, A. Mehmanparast, A. Kolios, I. Tavares, Corrosion fatigue crack growth mechanisms in offshore monopile steel weldments, *Fatigue Fract. Eng. Mater. Struct.* 40 (2017) 1868–1881.
- [4] V. Igwezezie, A. Mehmanparast, A. Kolios, Materials selection for XL wind turbine support structures: a corrosion-fatigue perspective, *Mar. Struct.* 61 (2018) 381–397.
- [5] S.-P. Zhu, Q. Liu, W. Peng, X.-C. Zhang, Computational-experimental approaches for fatigue reliability assessment of turbine bladed disks, *Int. J. Mech. Sci.* 142 (2018) 502–517.
- [6] S.-P. Zhu, Y. Liu, Q. Liu, Z.-Y. Yu, Strain energy gradient-based LCF life prediction of turbine discs using critical distance concept, *Int. J. Fatigue* 113 (2018) 33–42.
- [7] S.-P. Zhu, Z.-Y. Yu, Q. Liu, A. Ince, Strain energy-based multiaxial fatigue life prediction under normal/shear stress interaction, *Int. J. Damage Mech* 1056789518786031 (2018).
- [8] H. Xin, M. Veljkovic, Fatigue crack initiation prediction using phantom nodes-based extended finite element method for S355 and S690 steel grades, *Eng. Fract. Mech.* 214 (2019) 164–176.
- [9] S. Charoenphan, Bank LC, M.E. Plesha, Progressive tearing failure in pultruded composite material tubes, *Compos. Struct.* 63 (2004) 45–52, [https://doi.org/10.1016/S0263-8223\(03\)00130-2](https://doi.org/10.1016/S0263-8223(03)00130-2).
- [10] Z. Liu, J. Correia, H. Carvalho, A. Mourão, A. De Jesus, R. Calçada, et al., Global-local fatigue assessment of an ancient riveted metallic bridge based on submodelling of the critical detail, *Fatigue Fract. Eng. Mater. Struct.* 42 (2019) 546–560.
- [11] J.D. Burk, F.V. Lawrence, Influence of bending stresses on fatigue crack propagation life in butt joint welds, *Weld. Res. Suppl.* 2 (1977) 61–66.
- [12] G.A. Webster, A.N. Ezeilo, Residual stress distributions and their influence on fatigue lifetimes, *Int. J. Fatigue* 23 (2002) 375–383, [https://doi.org/10.1016/S0142-1123\(01\)00133-5](https://doi.org/10.1016/S0142-1123(01)00133-5).
- [13] J. Burk, F. Lawrence, The Effect of Residual Stresses of Weld Fatigue Life, 1978.
- [14] K. Spyridoni, H. Xin, M. Hermans, M. Veljkovic, Calibration of welding simulation parameters of fillet welding joints used in the orthotropic steel deck, 14th Nord. Steel Constr. Conf., Copenhagen, Denmark, 2019.

- [15] H. Xin, M. Veljkovic, Effects of residual stresses on fatigue crack initiation of butt-welded plates made of high strength steel, *Seventh Int. Conf. Struct. Eng. Mechanics Comput.*, Cape Town, 2019.
- [16] M. Beghini, L. Bertini, Fatigue crack propagation through residual stress fields with closure phenomena, *Eng. Fract. Mech.* 36 (1990) 379–387.
- [17] T.L. Teng, C.P. Fung, P.H. Chang, Effect of weld geometry and residual stresses on fatigue in butt-welded joints, *Int. J. Press. Vessel. Pip.* 79 (2002) 467–482, [https://doi.org/10.1016/S0308-0161\(02\)00060-1](https://doi.org/10.1016/S0308-0161(02)00060-1).
- [18] T.L. Teng, P.H. Chang, Effect of residual stresses on fatigue crack initiation life for butt-welded joints, *J. Mater. Process. Technol.* 145 (2004) 325–335, <https://doi.org/10.1016/j.jmatprotec.2003.07.012>.
- [19] Y. Dong, Y. Garbatov, Soares C. Guedes, Fatigue crack initiation assessment of welded joints accounting for residual stress, *Fatigue Fract. Eng. Mater. Struct.* 41 (2018) 1823–1837, <https://doi.org/10.1111/ffe.12824>.
- [20] X.-K. Zhu, J.A. Joyce, Review of fracture toughness (G, K, J, CTOD, CTOA) testing and standardization, *Eng. Fract. Mech.* 85 (2012) 1–46.
- [21] G.R. Irwin, Analysis of stresses and strains near the end of a crack traversing a plate, *J. Appl. Mech. Trans. ASME E24* (1957) 351–369.
- [22] G.R. Irwin, Onset of Fast Crack Propagation in High Strength Steel and Aluminum Alloys, Naval Research Lab, Washington DC, 1956.
- [23] A.A. Griffith, VI. The phenomena of rupture and flow in solids, *Philos Trans R Soc London Ser A, Contain Pap a Math or Phys Character* 221 (1921) 163–198.
- [24] P.C. Paris, M.P. Gomez, W.E. Anderson, A Rational Analytical Theory of Fatigue, *The Trend in Engineering*, 13, U Washington, Seattle, WA, 1961.
- [25] R.O. Ritchie, Near-Threshold Fatigue Crack Propagation in Ultra-High Strength Steel: Influence of Load Ratio and Cyclic Strength, 1976.
- [26] R.G. Forman, V.E. Kearney, R.M. Engle, Numerical analysis of crack propagation in cyclic-loaded structures, *J. Basic Eng.* 89 (1967) 459–463.
- [27] S. Suresh, G.F. Zamiski, D.R.O. Ritchie, Oxide-induced crack closure: an explanation for near-threshold corrosion fatigue crack growth behavior, *Metall. Mater. Trans. A* 12 (1981) 1435–1443.
- [28] W. Elber, The significance of fatigue crack closure, *Damage Toler. Aircr. Struct. ASTM International*, 1971.
- [29] R.O. Ritchie, Mechanisms of fatigue-crack propagation in ductile and brittle solids, *Int. J. Fract.* 100 (1999) 55–83.
- [30] A.M.P. De Jesus, R. Matos, B.F.C. Fontoura, C. Rebelo, L. Simões Da Silva, M. Veljkovic, A comparison of the fatigue behavior between S355 and S690 steel grades, *J. Constr. Steel Res.* 79 (2012) 140–150, <https://doi.org/10.1016/j.jcsr.2012.07.021>.
- [31] Abaqus V. 6.14 Documentation, Dassault Syst Simulia Corp 2014.
- [32] N. Moës, J. Dolbow, T. Belytschko, A finite element method for crack growth without remeshing, *Int. J. Numer. Methods Eng.* 46 (1999) 131–150.
- [33] J.R. Rice, A path independent integral and the approximate analysis of strain concentration by notches and cracks, *J. Appl. Mech.* 35 (1968) 379–386.
- [34] J.W. Hutchinson, Singular behaviour at the end of a tensile crack in a hardening material, *J. Mech. Phys. Solids* 16 (1968) 13–31.
- [35] Rice Jr, G.F. Rosengren, Plane strain deformation near a crack tip in a power-law hardening material, *J. Mech. Phys. Solids* 16 (1968) 1–12.
- [36] A.S. Kobayashi, S.T. Chiu, R. Beeuwkes, A numerical and experimental investigation on the use of J-integral, *Eng. Fract. Mech.* 5 (1973) 293–305.
- [37] ASTM E, 647: standard test method for measurement of fatigue crack growth rates, *Annu B ASTM Stand* 3 (2011) 591–630.
- [38] Standardization IO for. *Metallic Materials: Fatigue Testing: Fatigue Crack Growth Method. ISO 12108. ISO; 2002.*
- [39] International A, ASTM E2472–12 Standard Test Method for Determination of Resistance to Stable Crack Extension under Low-Constraint Conditions, 2012.
- [40] U. Zerbst, M. Heinemann, C. Dalle Donne, D. Steglich, Fracture and damage mechanics modelling of thin-walled structures—an overview, *Eng. Fract. Mech.* 76 (2009) 5–43.
- [41] D.J. Horsley, Background to the use of CTOA for prediction of dynamic ductile fracture arrest in pipelines, *Eng. Fract. Mech.* 70 (2003) 547–552.
- [42] I. Boko, N. Torić, B. Peroš, Fire resistance analysis of steel structures, *Gradjevinar* 64 (2012) 631–640.
- [43] EN 1993-1-2:2008, Eurocode 3: Design of Steel Structures - Part 1-2: General Rules Structural Fire Design, CEN, Brussels, 2008.